

Improved charge transfer through the minimal addition of Pb as a sintering aid to TiO₂-based low-temperature dye sensitised solar cell

Hazim Khir^a, A. K. Pandey^{a,b,*}, R. Saidur^{a,f}, Muhammad Shakeel Ahmad^c, Nasrudin Abd Rahim^c, M. Dewika^d, M. Samykan^e

^aResearch Centre for Nanomaterials and Energy Technology (RCNMET), School of Engineering & Technology, Sunway University, No. 5, Jalan Universiti, Bandar Sunway, Petaling Jaya, 47500 Selangor Darul Ehsan, Malaysia

^bSunway Materials Smart Science and Engineering (SMS2E) Research Cluster, Sunway University, No. 5 Jalan Universiti, Bandar Sunway, Petaling Jaya 47500, Selangor, Malaysia

^cHigher Institution Centre of Excellence (HiCoE), UM Power Energy Dedicated Advanced Centre (UMPEDAC), Level 4, Wisma R&D, University of Malaya, Jalan Pantai Baharu, 59990 Kuala Lumpur, Malaysia

^dCentre of American Education, Sunway University, No. 5, Jalan Universiti, Bandar Sunway, Petaling Jaya, 47500 Selangor Darul Ehsan, Malaysia

^eCollege of Engineering, University Malaysia Pahang, Lebuhraya Tun Razak, 26300 Gambang, Kuantan, Pahang, Malaysia

^fSchool of Engineering, Lancaster University, LA1 4YW, United Kingdom

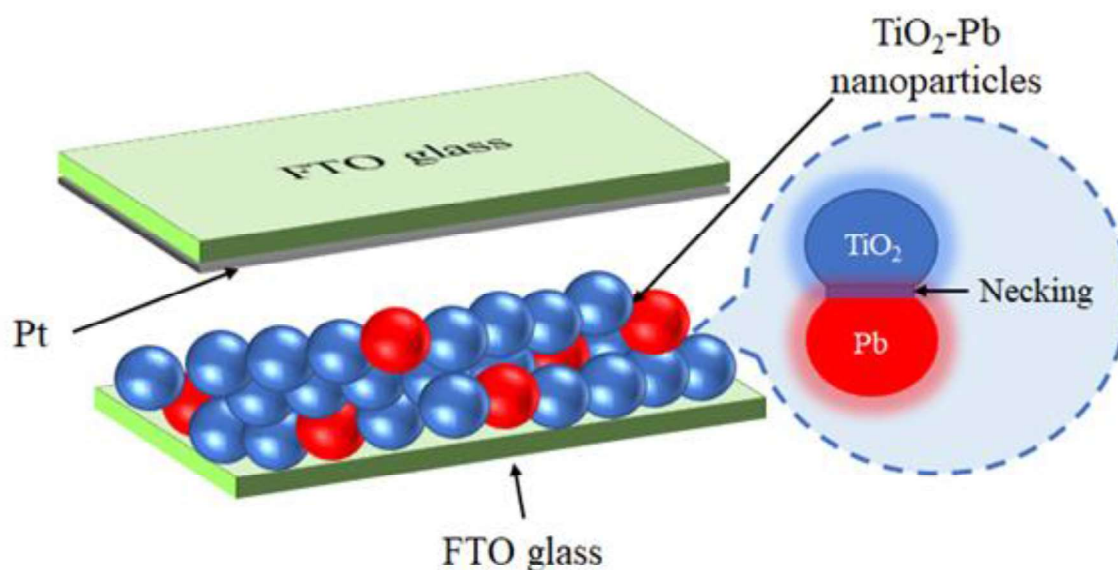
Abstract

The poor interparticle connectivity between the nanoparticles architecture of photoanode due to insufficient sintering temperature has been an issue for developing flexible dye sensitised solar cell (DSSC). This issue has led flexible DSSC to yield low conversion efficiency. This research aims to implement lead (Pb) as sintering aid to improve the interparticle connection of the photoanode by using the concept of liquid phase sintering. With low melting point of Pb (327.5°C), necks were formed at the titanium dioxide (TiO₂)-Pb interface that improved the connection and lowered the electronic resistance even at low sintering temperature of 150-250°C. Morphological studies showed the formation of these necks, while phase analysis indicated the more desirable TiO₂ anatase phase was present. Specimens containing 5wt% Pb in the TiO₂ matrix showed the highest efficiency value of 8.73% at 250°C, which is even higher compared to their high-temperature (450°C) counterpart by 12.21%. This is due to surface fusion of Pb at a lower temperature, leading to enhanced interparticle contact and reduction in recombination reactions. Further increase in Pb did not improve the conversion efficiency which can be due to high charge trapping sites and layer cracking due to high amounts of Pb in TiO₂ matrix.

Keywords: Flexible DSSC; photoanode; TiO₂; sintering; low temperature

* Corresponding author: Email (s): adarsh.889@gmail.com; adarshp@sunway.edu.my (A. K. Pandey)

Graphical abstract



Highlights

- Lowered resistance and improved connection due to neck formation between TiO₂-Pb
- Sintering of photoanode at low temperatures (150°C, 200°C and 250°C)
- 12.21% enhancement of DSSC efficiency with Pb sintering aid
- 5wt% Pb in the TiO₂ matrix showed the highest efficiency value of 8.73%

Contents

| | |
|---|----|
| 1.0 Introduction..... | 3 |
| 2.0 Methodology | 6 |
| 2.1 Materials | 6 |
| 2.2 Preparation of Pb sintering aid | 6 |
| 2.3 Preparation of photoanode samples | 6 |
| 2.4 Fabrication of DSSC devices..... | 6 |
| 2.5 Characterisation and analysis process | 7 |
| 3.0 Results and discussion | 7 |
| 3.1 Morphological studies..... | 7 |
| 3.2 Light absorption studies | 11 |
| 3.3 Electron transfer studies | 12 |
| 3.4 I-V curve | 16 |
| 4.0 Conclusions..... | 20 |
| References..... | 21 |

1.0 Introduction

Dye sensitised solar cells (DSSCs) are a third-generation solar cell that have been growing in popularity due to their low cost of production with readily available materials, easy fabrication process, ability to operate under low-light conditions, good stability, and nice aesthetics [1,2]. DSSC is a sandwich structure comprised of components including the conductive substrate, photoanode, counter electrode, sensitizer/dye and electrolyte. Typically, the conductive substrate is made up of conductive glass materials such as fluorine tin oxide (FTO) glass with one substrate coated with semiconducting materials such as titanium dioxide (TiO_2) nanoparticles that are sensitised with dyes (ruthenium-based) [3]. Meanwhile, the other substrate is coated with counter electrode catalysts, typically platinum or other materials such as MXene (Ti_3C_2) flakes [4] and tungsten disulfide (WS_2) nanosheets [5]. The two electrodes are then joined together with some iodide-triiodide liquid electrolyte is usually deposited in between them to complete the device. Due to the device's simplicity, DSSC have been under intensive research, with the highest efficiency recorded at 14.2% in the year 2020 [6], a slight increase from the previous record of 12.3% in 2011 [7]. The lack of significant improvement in the efficiency of DSSC highlights their main issue, especially when compared to some other third-generation solar cells, such as perovskite and organic solar cells with conversion efficiency of 25.5% and 19%, respectively [8,9]. Therefore, researchers have been taking a different approach by reducing the cost of DSSC manufacturing instead while still producing good or comparable efficiency.

The cost of DSSC manufacturing can be decreased by developing flexible DSSC using flexible materials such as plastic substrate made up of indium tin oxide-polyethyleneterephthalate (ITO-PET) and indium tin oxide-polyethylenenaphtalate (ITO-PEN). These materials are flexible, lightweight, have good transmittance and conductivity with low production cost by utilising roll-to-roll system to mass produce the substrate in industry [10,11]. The ability of these materials to be shaped easily allowed them to be applicable for mobile and wearable applications, encouraging the development of flexible DSSC even further [12]. Despite all the advantages of the flexible DSSCs, these devices suffer from low conversion efficiency compared to rigid glass-based DSSCs with the highest efficiency is reported at 10.28% [13].

A typical rigid glass-based DSSC underwent sintering at high temperature (usually 450°C for TiO_2 photoanode) to improve the interparticle connection between the photoanode nanoparticles, remove organic surfactant in the photoanode paste and enhance the adhesion between the photoanode and substrate [14]. However, this approach is not applicable for

1 plastic-based DSSC with low thermal stability as the ITO-PET and ITO-PEN polymer substrate
2 would deform at temperature higher than 150°C [11]. Hence, various research has been
3 conducted to enhance the efficiency of DSSC at low sintering temperature.
4

5 One of the approaches that have been taken to enhance the efficiency of DSSC is doping
6 the photoanode with metallic cations materials by tuning the band structure of the photoanode
7 [15]. By adding tin (Sn) as dopant to TiO₂ photoanode, Ni et al. [16] managed to develop DSSC
8 with good conversion efficiency of 8.75% compared to DSSC with undoped TiO₂ (7.46%).
9 This was attributed to the Sn dopant that expands the electron mobility and raises the flat band
10 potential, eventually improved the performance of DSSC. Dubey et al. [17] meanwhile studied
11 a variety of dopants such as vanadium (V), iron (Fe), chromium (Cr) and cobalt (Co) to TiO₂
12 photoanode, which produced DSSC with efficiency of 3.33%, 4.85%, 3.29% and 3.20%
13 respectively compared to pure TiO₂ (1.31%). Thus, highlighting the effectiveness and potential
14 in using dopants as there are wide availability of materials that can still be studied. Dopants
15 have also shown to be effective for flexible DSSC that was sintered at low temperature of
16 130°C. This was demonstrated by Song et al. [18] where magnesium (Mg) was used as doping
17 material to TiO₂ photoanode. An increase in efficiency can be seen as Mg-doped TiO₂ DSSC
18 yielded an efficiency of 2.2% compared to undoped ones (1.7%) due to the change in the
19 conduction band state of TiO₂ surface.
20
21
22
23
24
25
26
27
28
29
30
31

32 By using the surface plasmon resonance effects found in metallic nanoparticles and the
33 concept of liquid phase sintering, another approach can also be taken to improve the DSSC
34 sintering process. Liquid phase sintering utilises at least two chemical elements mixed at
35 different compositions, with the major component remaining as solid while the minor
36 component becomes the aids that forms liquid during sintering [19]. Liquid phase sintering
37 enhances the sintering mechanism by enhancing the diffusion speed and mass transfer
38 mechanism. Ahmad et al. [20] utilises germanium (Ge) as sintering aid to TiO₂ photoanode,
39 where they discovered necks were formed at the TiO₂-Ge interface during sintering. These
40 necks helped improve the interparticle connection leading to better efficiency from 4.03% for
41 pure TiO₂ photoanode to 5.65% with the addition of Ge sintering aid. In another study, Ahmad
42 et al. [21] applied zinc (Zn) nanoparticles as sintering aid to TiO₂ nanoparticles with lower
43 sintering temperature of 200°C. A similar outcome was obtained with necks forming at the
44 TiO₂-Zn interface, improving the efficiency from 4.27% for pure TiO₂ photoanode sintered at
45 450°C, to 4.92%. Due to the low melting point of Zn (419.5°C), the necks were formed despite
46 the low sintering temperature because of the rules of metallurgical sintering. In metallurgical
47
48
49
50
51
52
53
54
55
56
57
58
59
60
61
62
63
64
65

1 sintering, the sintering temperature of metals are typically found at around 67-75% of the
2 metals' melting point [22]. Hence, addition of sintering aid for liquid phase is suitable for both
3 high and low temperature DSSC development.
4

5 Lead (Pb) has high durability, density and is a corrosion resistant metal with a low
6 melting point of 327.5°C [23]. Pb is a group IV element similar to Ge and Sn which have shown
7 good photocatalytic activity with TiO₂ has encouraged some previous studies to try reproduce
8 similar outcomes. Pb was used as dopant material with TiO₂ that has tuned the energy bandgap
9 and electronic structure of TiO₂, extending the wavelength response for solar light, increasing
10 the number of photogenerated electrons and enhances the photocatalytic activity of Pb-doped
11 TiO₂ films [24,25]. Lead sulphide (PbS) nanoparticles with their tuneable band gap have been
12 used as photoanode material for DSSC in a study by Mishra & Saha [26] with power conversion
13 efficiency (PCE) of 1.92%. PbS has also been used with TiO₂ photoanode to form
14 nanocomposite paste in a study by Singh et al. [27] which produced DSSC with efficiency of
15 0.35%, compared to the pure TiO₂ photoanode (0.08%).
16
17

18 Overall as can be seen from the above literature review, yet extensive studies have not
19 been conducted using pure Pb metal nanoparticles in DSSC development. Besides, the
20 implementation of metal nanoparticles as sintering aid to DSSC photoanode has still not been
21 a widely research topic in this field. However, metal type of nanoparticles have great potential
22 to enhance the power conversion efficiency (PCE) of DSSCs especially for low temperature
23 applications. Thus, this research aims to develop highly efficient DSSC at low sintering
24 temperature with novel implementation of Pb as sintering aid to TiO₂ photoanode. The low
25 melting point and high charge carrier mobility would make them a suitable sintering aid to
26 form necks with the TiO₂ nanoparticles despite the low sintering temperature [23]. Several
27 different compositions of Pb and low sintering temperatures are investigated to study their
28 effects on the performance of DSSC as well as determining the optimal condition. Highest PCE
29 (8.73%) is found to be for specimens containing 5wt% Pb in the TiO₂ matrix at 250°C which
30 outperform as compared to their high-temperature (450°C) counterpart (having PCE of 7.78%
31) by 12.21%. Besides, the low cost of Pb due to the abundance of the material is another key
32 factor in supporting the viability of this novel research to develop low cost DSSC with good
33 efficiency.
34
35
36
37
38
39
40
41
42
43
44
45
46
47
48
49
50
51
52
53
54
55
56
57
58
59
60
61
62
63
64
65

2.0 Methodology

2.1 Materials

Titania (TiO₂) paste (Sigma-Aldrich), fluorine tin oxide (FTO) glass (Sigma-Aldrich, surface resistivity: 13Ω/sq), Pb powder (Sigma-Aldrich, 100 mesh), platinum (Pt)-coated FTO glass (Solaronix), iodolyte An-50 (Solaronix), ruthenizer 535-bisTBA (Solaronix), methanol (Fisher Scientific), acetonitrile (Fisher Scientific), ethanol (Fisher Scientific), binder clips.

2.2 Preparation of Pb sintering aid

20g of Pb powder (100 mesh) was deposited into a grinding bowl with zirconia balls for the grinding process using a planetary ball mill (Fritsch Pulverisette 5) operated at 500 rpm. Multiple grinding cycles were conducted until the Pb powder was found to be in nanoparticle size of around 450-500 nm, checked by using a particle size analyser (Anton Paar Lifesizer 500).

2.3 Preparation of photoanode samples

Pure FTO glass was cleaned using methanol each time before they were deposited with photoanode materials. A coating area of 1cm x 1cm was prepared by taping up some parts of the FTO glass using cellophane tape. Pure TiO₂ photoanode samples were prepared by depositing some TiO₂ paste onto the coating area and was coated via doctor blade method. The coated sample was left to dry for 1 hour before the tape was removed, leaving a smooth coated surface. The coated FTO glass was then placed onto a hotplate (IKA RCT basic) and was heated at several different temperature (150°C, 200°C, 250°C and 450°C) for 3 hours. After the sintering process, the samples were then kept and secured for the next steps.

In order to prepare the Pb-TiO₂ photoanode samples, different amount of grinded Pb powder was added to the TiO₂ paste and mixed to form different weight composition of Pb (0.5wt%, 1wt%, 3wt%, 5wt% and 10wt%). Similar to the previous step, the doctor blade method was used to coat the composite paste onto the FTO glass to form a coating area of 1cm x 1cm. The samples were then heated at different temperatures (150°C, 200°C and 250°C) for 3 hours. The sintered photoanode samples were then kept and secured for further use.

2.4 Fabrication of DSSC devices

Ruthenium-based dye solution was prepared by dissolving 10mg of ruthenizer powder into 5ml of acetonitrile solution. The photoanode sample was soaked into the dye solution and left inside for 1 day. After 24 hours, the photoanode sample was taken out from the dye solution and was left to dry at room temperature for 5 hours. Pt-coated FTO glass was then combined

1 together with the dyed photoanode sample. A drop of electrolyte was deposited into the sample
2 via a small hole on the Pt-coated FTO glass to complete the device. Binder clips were then used
3 to clip the two components together. Similar process was repeated for all the photoanode
4 samples and the devices were then kept for further use.
5
6
7
8
9

10 **2.5 Characterisation and analysis process**

11 Several characterisation studies were conducted on the photoanode samples using
12 equipment such as the field emission scanning electron microscope (FESEM model: Hitachi
13 SU8010) and transmission electron microscope (TEM model: FEI Tecnai G2 20 S-TWIN) for
14 morphological studies. Elemental composition and mapping of the photoanode samples were
15 also investigated using the scanning electron microscope-energy dispersive x-ray (SEM-EDX
16 model: TESCAN VEGA 3) analysis. Phase analysis was also conducted using x-ray diffraction
17 (XRD) analysis (XRD model: Rigaku Miniflex 600). Light absorption studies were also
18 conducted using UV-visible spectroscopy (UV-vis model: PerkinElmer Lambda 750).
19 Electrochemical impedance spectroscopy (EIS) analysis was also conducted using Gamry
20 Interface 1010E Potentiostat to plot the Nyquist and Bode plot. Nyquist plot was used to check
21 for the series (R_s) and charge transfer resistance (R_{CT}) while the Bode plot was applied to
22 determine the electron lifetime (t) of the DSSC devices. The frequency range was set at 0.1 Hz
23 – 1 MHz and the voltage were set at 10 mV for all samples. Solar simulator (solar simulator
24 model: IVT 300) was also used to measure the current-voltage (I-V) curves, short circuit
25 current (J_{sc}), open circuit voltage (V_{oc}), fill factor (FF) and power conversion efficiency
26 (PCE). A 1600W Xenon lamp (SAN-EI electric Co., Ltd) was used in IVT 300 series solar
27 simulator . The calibration was done before testing using a certified golden solar cell
28 (Amorphous Silicon solar cell). The reason behind using a standard Amorphous Si solar cell it
29 was due to minimum mismatch. The mismatch was found to be approximately 3.7% and for
30 proper measurements it was adjusted in machine parameters as a mismatch factor. The data
31 obtained were then analysed and tabulated accordingly in the research. At least 5 samples for
32 each selected sample have been tested and the average value has been presented in this study.
33
34
35
36
37
38
39
40
41
42
43
44
45
46
47
48
49
50
51

52 **3.0 Results and discussion**

53 **3.1 Morphological studies**

54 FESEM equipment have been used to capture the image of the prepared photoanode
55 samples to analyse their morphologies at different sintering temperatures and with the addition
56
57
58
59
60
61
62
63
64
65

of Pb sintering aids. Figure 1 shows the coated and sintered photoanode samples on top of FTO glasses were used for the FESEM analysis as well as the elemental mapping and composition via the SEM-EDX analysis.

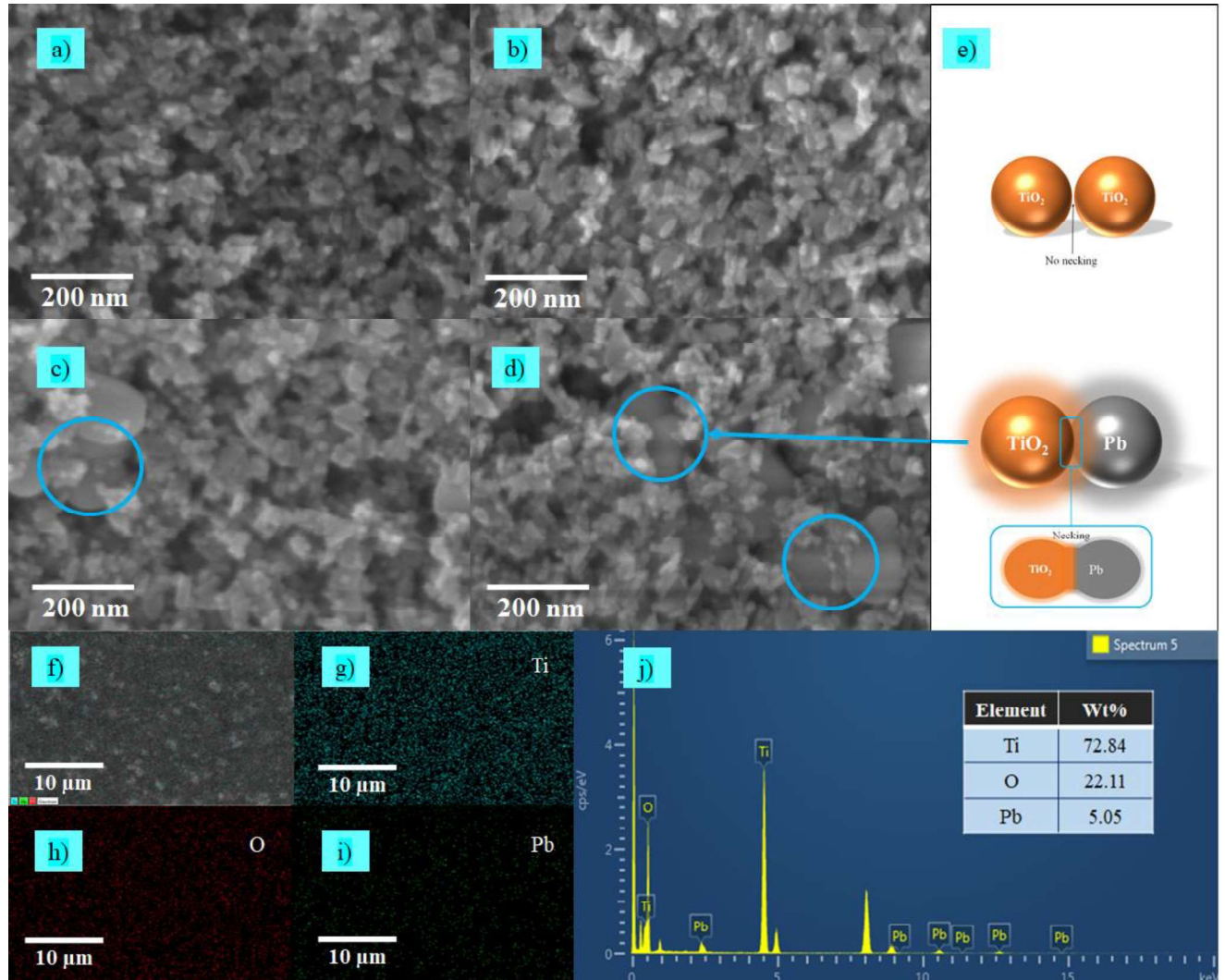


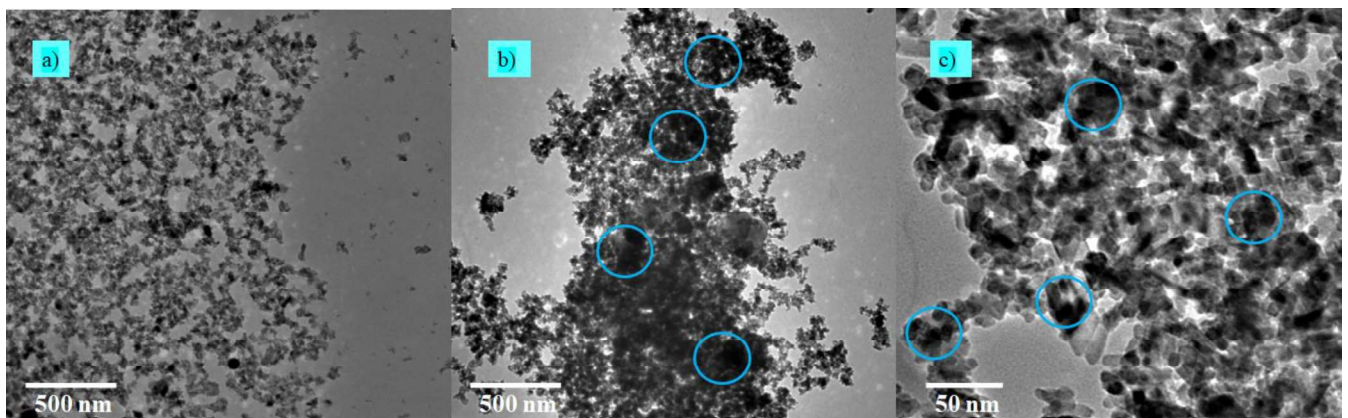
Figure 1: a) FESEM image of pure TiO_2 photoanode sintered at 150°C b) FESEM image of pure TiO_2 photoanode sintered at 250°C c) FESEM image of TiO_2 -5% Pb photoanode sintered at 200°C d) FESEM image of TiO_2 -5% Pb photoanode sintered at 250°C e) Schematic diagram of the necking between the TiO_2 -Pb nanoparticles f)-i) SEM-EDX elemental mapping for Ti, O and Pb elements respectively j) EDX report for TiO_2 -5% Pb photoanode sample

FESEM images of the prepared photoanode samples have been depicted in Figure 1a-d. The effect of sintering temperature can be observed from the FESEM images, where the porosity of the films seems to have increased as the sintering temperature increased. The TiO_2

1 nanoparticles in Figure 1b have also agglomerated more with a denser arrangement than the
2 nanoparticles in Figure 1a due to the increase in sintering temperature. The increase in sintering
3 temperature has enlarged the surface area for better dye absorption, light harvesting and
4 eventually DSSC performance.
5

6
7 Meanwhile, Figures 1c and 1d highlight the presence of Pb sintering aids in the
8 photoanode films. The TiO₂ nanoparticles in both figures have shown better connectivity due
9 to the presence of Pb sintering aid as indicated in the figure. The cause for this improved
10 connection can be attributed to the aforementioned liquid phase sintering and metallurgical
11 sintering theory. Pb nanoparticles have been melted during the sintering process due to their
12 low melting point of 327.5°C. Since the sintering temperature of metal nanoparticles is
13 typically around 70% of their melting point, Pb nanoparticles were sintered well at 250°C [22].
14 The melting of Pb nanoparticles then caused the formation of necks at the TiO₂-Pb interface as
15 shown in Figure 1e, which would enhance the interparticle connectivity of the photoanode. The
16 presence of Pb nanoparticles with the desired elemental composition was also observed in the
17 EDX report of the TiO₂-5% Pb photoanode sample. Elemental mapping for the aforementioned
18 photoanode sample has also been conducted showing the presence of all the elements required
19 in the formation of necks at the TiO₂-Pb interface. The absence of other elements in the EDX
20 analysis indicates that there were no traces of impurities in the prepared photoanode samples.
21 Hence, highlighting the preparation of photoanode samples have been prepared accordingly in
22 the research.
23
24

25
26
27
28
29
30
31
32
33
34
35
36
37 Besides FESEM analysis, TEM analysis was also conducted and their images were also
38 observed to study the morphologies of the photoanode samples prepared as shown in Figure 2.
39



55
56
57
58
59
60
61
62
63
64
65

Figure 2: TEM images of photoanode samples a) pure TiO₂ sintered at 250°C b) TiO₂-5% Pb sintered at 250°C with lower magnification c) TiO₂-5% Pb sintered at 250°C with higher magnification

Figure 2 showed the TEM images of photoanode samples prepared at 250°C with and without the addition of Pb sintering aid. The effect of the implementation of Pb sintering aid can clearly be seen in Figure 2b & 2c where there has been an increase in the aggregation between the nanoparticles with the formation of larger chunks of nanoparticles. The highlighted section in Figure 2b & 2c indicates the formation of necks between the TiO₂-Pb nanoparticles during the sintering process. The presence of these nanoparticle aggregations in the TEM images further supports the observation made in the FESEM images regarding the formation of necks that improve the interparticle connection.

Phase identification of photoanode samples has been conducted via the XRD analysis as shown in Figure 3.

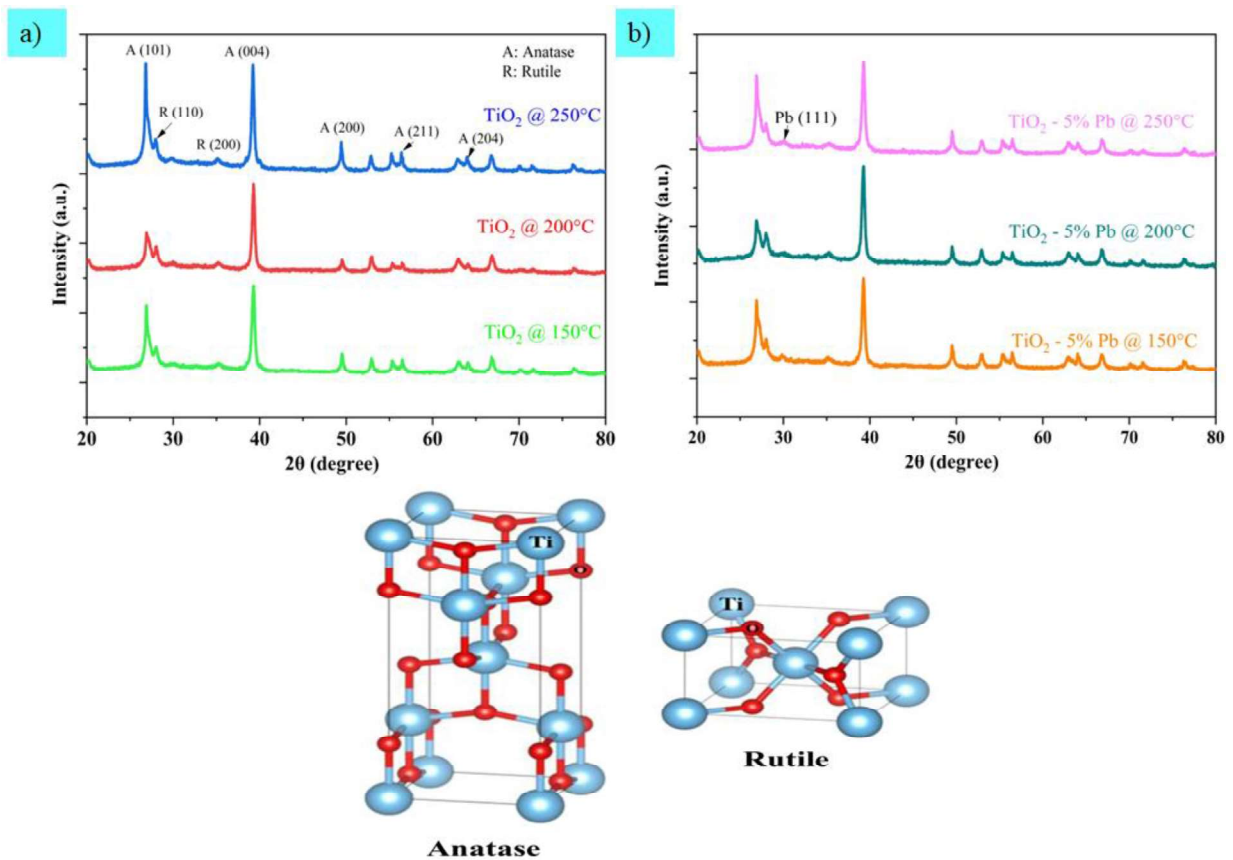


Figure 3: a) XRD analysis of pure TiO₂ photoanode samples at multiple sintering temperature b) XRD analysis of TiO₂ - 5%Pb photoanode samples at multiple sintering temperature with unit cells of anatase TiO₂ and rutile TiO₂ [28]

Figure 3a indicates that the peaks have been formed at similar areas for each photoanode sample even with different sintering temperatures. This observation shows that the crystallite structure of TiO₂ did not experience any phase change despite the different sintering temperatures. The more desirable TiO₂ anatase phase have been found to be more prevalent

1
2
3
4
5
6
7
8
9
10
11
12
13
14
15
16
17
18
19
20
21
22
23
24
25
26
27
28
29
30
31
32
33
34
35
36
37
38
39
40
41
42
43
44
45
46
47
48
49
50
51
52
53
54
55
56
57
58
59
60
61
62
63
64
65

than the less desirable rutile phase as highlighted in the peaks shown in Figure 3a. Peaks were formed at 2θ positions of 26° , 39° , 49° , 56° and 64° with miller indices of (101), (004), (200), (211) and (204) planes, respectively, indicating TiO₂ anatase phase [29]. Meanwhile, a few peaks formed at 27° and 36° with miller indices of (110) and (200) planes, respectively which indicated the TiO₂ rutile phase. The unit cells showed that the Ti-Ti distance is longer, while the Ti-O distance is shorter in anatase phase compared to the rutile phase. This structure would then cause a difference in the mass densities and electronic band structures [30]. Hence, anatase TiO₂ have larger bandgap, higher surface energy, lower recombination reaction and smaller grain size, for better photocatalytic and photovoltaic activity [29,31]. These advantages would eventually lead to a higher DSSC efficiency, making TiO₂ anatase phase more favorable. Pb sintering aid has also been found to not have caused a change in the TiO₂ phase. TiO₂ anatase have remained dominant despite adding Pb as indicated by the peaks formed at 32° with miller indices (111) plane as shown in Figure 3b [32]. From these observations, it can be deemed that the low sintering temperature of 150-250°C as well as with the addition of Pb nanoparticles as sintering aid were suitable for maintaining good TiO₂ anatase phase.

3.2 Light absorption studies

Light absorption studies for the photoanode materials have been conducted by dissolving an appropriate amount of TiO₂, Pb, and TiO₂-5% Pb into ethanol solvent before they were sonicated for 30 minutes. Pure ethanol solution was then used as a reference, and the outcome from the UV-visible spectroscopy was shown in Figure 4. From the UV-vis spectra, the absorbance peak for TiO₂ sample was at the wavelength of 350 nm. This falls under the UV region as shown in Figure 4, typical for TiO₂ nanoparticles [33]. Similar finding was also obtained for the TiO₂-5% Pb sample where the absorbance peak was formed at a wavelength of 340 nm, also falling in the UV region. The presence of Pb particle can also be found in the nanocomposite with the formation of peak at around 270 nm, similar to the Pb sample. Apart from that, it can be seen that there was higher absorbance for the nanocomposite sample as opposed to pure TiO₂ and Pb sample. The addition of Pb nanoparticles was observed to have helped increase the absorbance of TiO₂-5% Pb sample even beyond the UV region. This was proven by the absorbance peak has been formed at the near-infrared region with wavelength of 870 nm, similar to the peak formed by the pure Pb nanoparticle as shown in Figure 4. Hence, indicating the impact of adding Pb nanoparticles as sintering aid to add wavelength response in the near-infrared region for the TiO₂-Pb nanocomposite sample. The improvement in the nanocomposite sample to absorb light at both UV and near-infrared region would help boost

1
2
3
4
5
6
7
8
9
10
11
12
13
14
15
16
17
18
19
20
21
22
23
24
25
26
27
28
29
30
31
32
33
34
35
36
37
38
39
40
41
42
43
44
45
46
47
48
49
50
51
52
53
54
55
56
57
58
59
60
61
62
63
64
65

their light absorption capabilities. This would eventually enhance the conversion efficiency of the solar device and encourage the implementation of Pb as sintering aid.

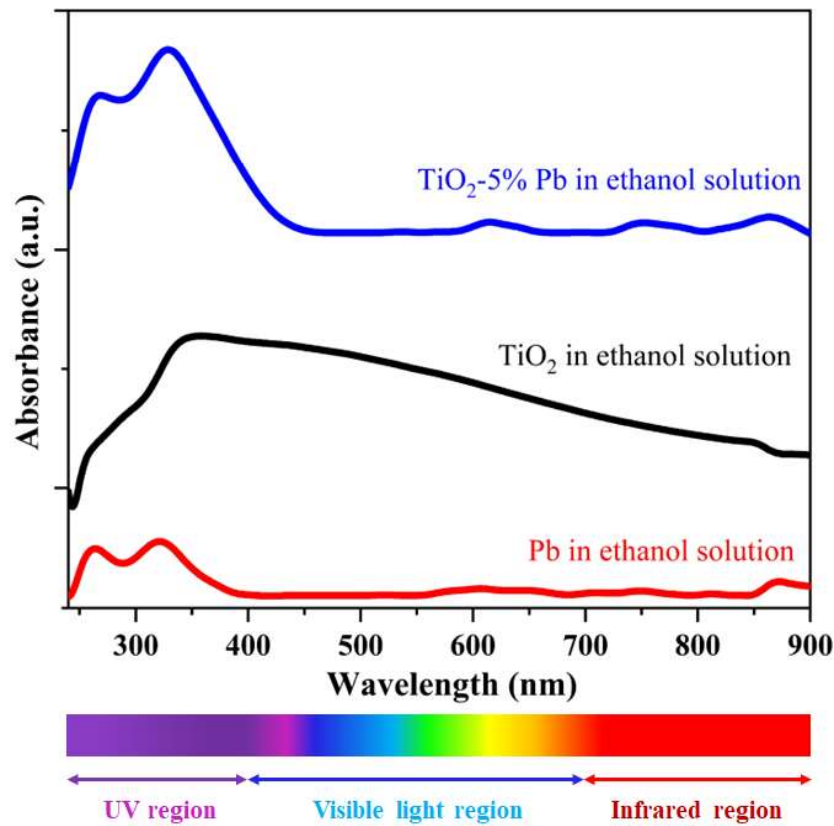


Figure 4: UV-visible spectra of Pb, TiO₂ and TiO₂-5% Pb in ethanol solution

3.3 Electron transfer studies

Figure 5 and 6 depicts the Nyquist and Bode plot from EIS analysis which was performed to study the electron transfer of the complete DSSC devices. EIS response for DSSC devices prepared at 250°C sintering temperature for different Pb composition have been studied. In theory, 250°C was determined to be the most suitable sintering temperature that would yield good results by considering the metallurgical sintering concept [22]. The effect of Pb composition was then studied by analysing the EIS response for these DSSC devices.

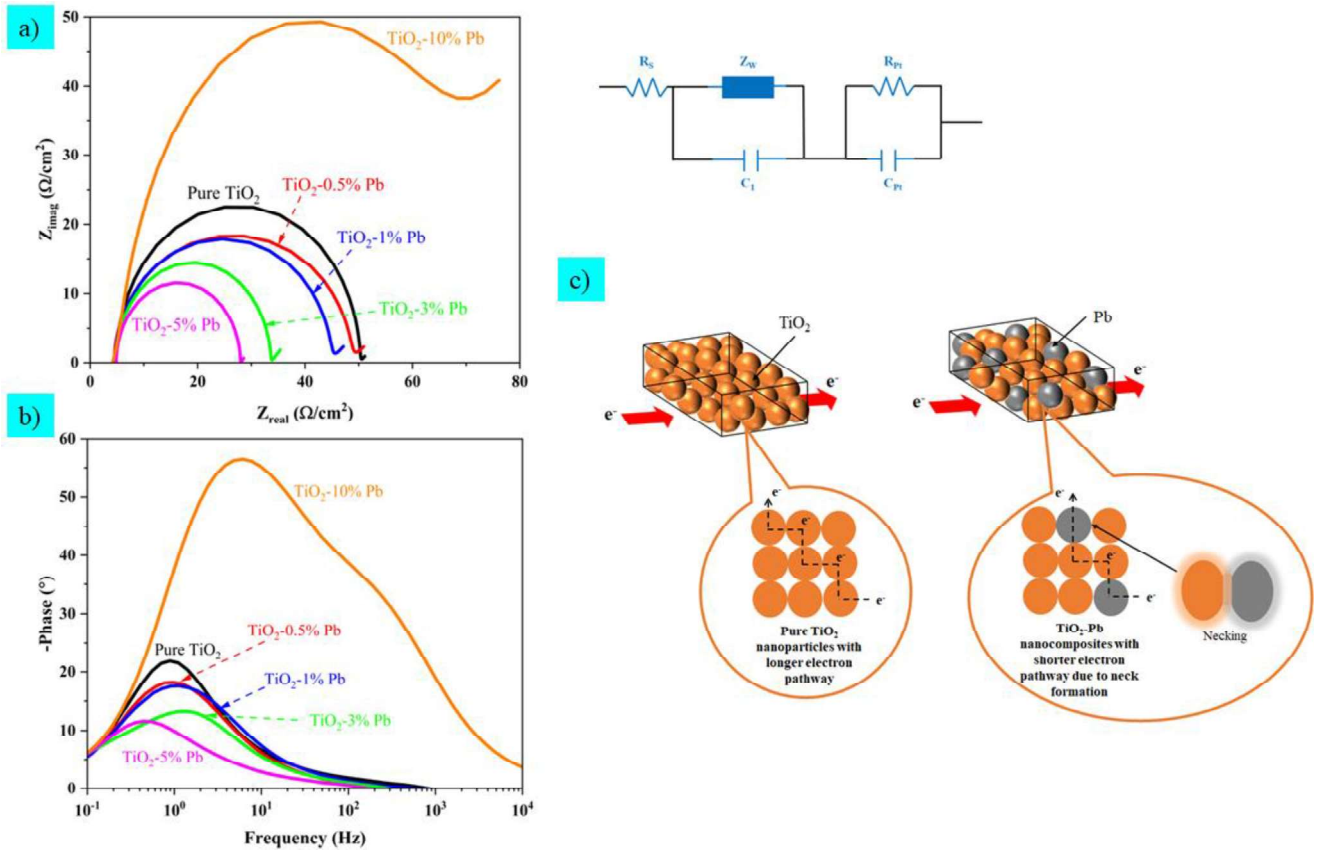


Figure 5: a) Nyquist plot for DSSC devices sintered at 250°C with equivalent circuit b) Bode plot for DSSC devices sintered at 250°C c) Schematic diagram of electron pathway between pure TiO_2 photoanode samples and TiO_2 -Pb composite photoanode sample

From the Nyquist plot, the charge transfer resistance (R_{CT}) of DSSC devices was observed to have decreased as Pb sintering aid was implemented to TiO_2 photoanode. The R_{CT} for DSSC based on pure TiO_2 photoanode was found to be $22.572 \Omega/\text{cm}^2$, while the R_{CT} for DSSC based on TiO_2 -0.5% Pb was $18.317 \Omega/\text{cm}^2$. The result indicated that the charge transfer capability of the composite photoanode was better. The improvement was attributed to the neck formation between the TiO_2 -Pb nanoparticles during the sintering process. The formation of these necks increased the interparticle connectivity from the surface fusion of Pb and the increase in electron density. This occurrence would then lead to shorter electron pathway for the transfer of electrons throughout the nanoparticles. With shorter electron pathway, the charge transfer would be improved and the charge transfer properties of the TiO_2 -Pb photoanode has been enhanced. Thus, the recombination reactions and resistance of DSSC devices have been reduced by adding Pb sintering aid as opposed to pure TiO_2 photoanode with higher resistance values. The R_{CT} was reduced even further as the composition of Pb was increased. The lowest R_{CT} value was discovered when TiO_2 -5% Pb photoanode was applied with a value of 11.54

1 Ω/cm^2 . However, the resistance was found to have increased when the composition of Pb was
2 increased to 10% with high R_{CT} value of $49.29 \Omega/\text{cm}^2$, higher than pure TiO_2 photoanode. This
3 occurrence was due to excessive amount of Pb, which became impurities that causes electron
4 trapping sites and surface defects [21].
5
6

7 The results from the Nyquist plot were supported even further with the study of Bode
8 plot. From Bode plot, the electron lifetime (t) of the DSSC devices was determined using
9 Equation (1) [17]:
10
11

$$12 \quad t \text{ (ms)} = \frac{1}{2\pi f_{max}} \quad (1)$$

13
14

15 Where, f_{max} is the maximum frequency from the Bode plot.
16

17 The t value for DSSC based on pure TiO_2 photoanode was calculated to be 179.229 ms while
18 the t value for DSSC based on TiO_2 -5% Pb photoanode was calculated to be 358.861 ms. The
19 longer the electron lifetime, the lower the possibility of recombination reactions to occur at the
20 TiO_2 network. With low charge transfer resistance, longer electron lifetime and less
21 possibilities of recombination reaction, TiO_2 -5% Pb has been concluded as the most suitable
22 composition for DSSC development. Meanwhile, TiO_2 -10% Pb composition was considered
23 unsuitable and worse than pure TiO_2 due to the high R_{CT} and low t (25.887 ms), with high
24 recombination reaction probability. Further analysis of DSSC fabricated using the TiO_2 -5% Pb
25 composition was then conducted to study the effect of sintering temperature.
26
27
28
29
30
31
32
33
34
35
36
37
38
39
40
41
42
43
44
45
46
47
48
49
50
51
52
53
54
55
56
57
58
59
60
61
62
63
64
65

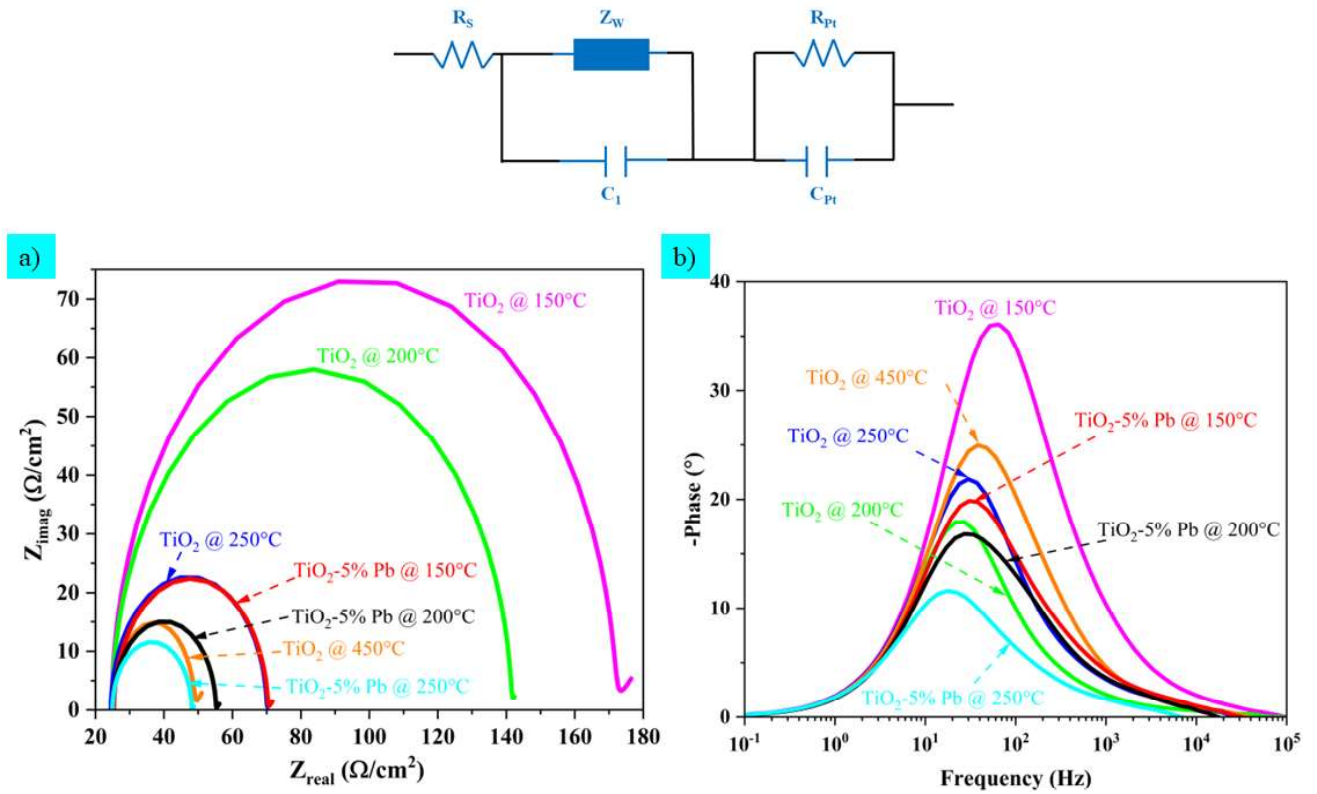


Figure 6: a) Nyquist plot for various DSSC devices with equivalent circuit b) Bode plot for various DSSC devices

EIS analysis for DSSC devices based on TiO_2 -5% Pb composition at different sintering temperature was conducted and compared with pure TiO_2 DSSC devices. Figure 6a showed that R_{CT} values decreased as the sintering temperature increases. The highest R_{CT} value was found for DSSC based on pure TiO_2 sintered at 150°C with a value of 72.966 Ω/cm². The photoanode's smaller porosity and surface area lowered the electrical contact between nanoparticles with low electron transfer that increased the resistance and recombination reaction [34]. To prevent such issue, TiO_2 photoanode is typically sintered at 450°C [35]. As shown in Figure 6a, the pure TiO_2 photoanode sintered at 450°C yielded lower R_{CT} value of 14.883 Ω/cm², highlighting the importance of having high sintering temperature. However, in this research, the photoanode samples with Pb addition were sintered at low temperature of 150°C-250°C to be applicable for flexible DSSC development [36].

Additionally, the absence of sintering aid also hindered the connection between the TiO_2 nanoparticles. Lower R_{CT} values (22.418 Ω/cm²) was obtained when 5% Pb was added, even at 150°C sintering temperature. The lowest R_{CT} value of 11.54 Ω/cm² was obtained when TiO_2 -5% Pb photoanode sintered at 250°C was implemented. The value was even lower than

1 the control DSSC based on TiO₂ photoanode sintered at 450°C ($R_{CT} = 14.883 \Omega/\text{cm}^2$). Due to
2 the concept of liquid phase and metallurgical sintering, Pb, with a melting point of 327.5°C,
3 has melted and formed necks at the TiO₂-Pb interface [19]. The interparticle connection of the
4 photoanode have been greatly enhanced, while the charge transfer resistance and
5 recombination reactions have been lowered. Besides the Nyquist plot, Bode plot have also been
6 analysed to calculate the electron lifetime of DSSC. The longest electron lifetime value was
7 obtained for DSSC based on TiO₂-5% Pb photoanode sintered at 250°C with a value of 358.861
8 ms. Thus, lowering the recombination reactions of the DSSC and lowering the resistance as
9 previously mentioned. From the EIS analysis, DSSC based on TiO₂-5% Pb photoanode sintered
10 at 250°C has demonstrated the potential to have the best performance.
11
12
13
14
15
16
17
18

19 **3.4 I-V curve**

20
21 The current-voltage (I-V) characteristics of the prepared DSSC devices have been
22 determined using a solar simulator and was plotted in Figure 7. From the solar cell I-V curve,
23 several important parameters in evaluating the performance of DSSC have also been calculated
24 and tabulated in Table 1. Dye loading for the DSSC was also performed via the absorption-
25 desorption method, and sodium hydroxide (NaOH)-ethanol solution was used to desorb the dye
26 loaded on the photoanode samples. The outcome of the dye loading was also presented in Table
27
28
29
30
31
32
33
34
35
36
37
38
39
40
41
42
43
44
45
46
47
48
49
50
51
52
53
54
55
56
57
58
59
60
61
62
63
64
65

1. Control DSSC device prepared with pure TiO₂ photoanode sintered at 450°C was used as reference, thus, comparisons can be made between the prepared and control DSSC.

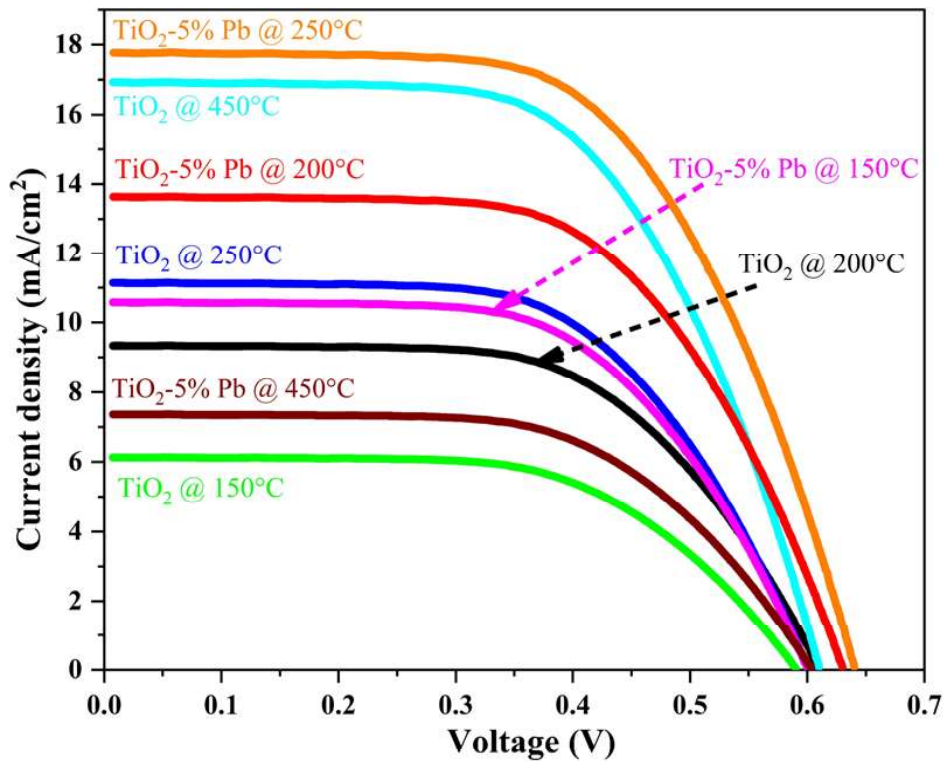


Figure 7: I-V curve for the prepared DSSC devices

Increased sintering temperature burned out more organic compounds and impurities in TiO₂ nanoparticles, which led to an enlarged surface area [34]. This then improved their dye loading capability, eventually enhancing their light harvesting capability. Meanwhile, improvement in the interparticle connection between the TiO₂ nanoparticles from the addition of Pb sintering aid have also shown to have improved the dye loading ability of the photoanode samples. The highest dye loading was obtained for the TiO₂-5% Pb photoanode sample sintered at 250°C with a value of $1.17 \times 10^{-7}/\text{cm}^2$, higher than the control DSSC sample. Thus, indicating that the prepared nanocomposite photoanode have good dye loading and light absorption capability that would eventually enhance the DSSC performance.

Table 1: Summary of parameters of DSSC samples

| Photoanode sample | Sintering temperature (°C) | PCE (%) | V _{oc} (V) | J _{sc} (mA/cm ²) | FF (%) | Dye loading ($\times 10^{-7}/\text{cm}^2$) |
|-------------------|----------------------------|---------|---------------------|---------------------------------------|--------|--|
| TiO ₂ | 150 | 2.70 | 0.59 | 6.13 | 56 | 1.01 |

| | | | | | | |
|------------------------------------|-----|------|------|-------|----|------|
| TiO₂ | 200 | 3.87 | 0.61 | 9.34 | 63 | 1.03 |
| TiO₂ | 250 | 4.48 | 0.60 | 11.14 | 71 | 1.03 |
| TiO₂ | 450 | 7.78 | 0.61 | 16.93 | 74 | 1.06 |
| TiO₂ - 5% Pb | 150 | 4.17 | 0.60 | 10.58 | 71 | 1.02 |
| TiO₂ - 5% Pb | 200 | 6.86 | 0.63 | 13.64 | 72 | 1.08 |
| TiO₂ - 5% Pb | 250 | 8.73 | 0.64 | 17.78 | 74 | 1.17 |
| TiO₂-5% Pb | 450 | 3.03 | 0.60 | 7.36 | 64 | n/a |

Table 1 shows that the open circuit voltage (V_{OC}) values for the samples underwent minimal changes and were slightly increased when Pb was added as a sintering aid. The values of V_{OC} depend on the difference between the Fermi energy level of photoanode and electrolyte's redox potential [37]. The short circuit current (J_{SC}) was discovered to have improved when the sintering temperature was increased and Pb sintering aid was added. The increased J_{SC} can be attributed to the enhanced dye absorption with higher charge transfer and lower recombination in the photoanode [15,37]. The increased interparticle contact, porosity and enlarged surface area from the increase in sintering temperature, have caused these changes, with high J_{SC} value of 16.93 mA/cm² obtained for DSSC sintered at 450°C. Meanwhile, the lowest J_{SC} (6.13 mA/cm²) was yielded by DSSC photoanode sintered at a low temperature of 150°C with a small surface area and low dye absorption. DSSC based on TiO₂-5% Pb photoanode sintered at a lower temperature of 250°C has also yielded the highest J_{SC} value. Thus, indicating that the presence of Pb nanoparticles has also improved the interparticle connectivity, dye absorption, and charge transfer. The recombination reaction has also been lowered as discussed in the EIS analysis. The fill factor (FF) of DSSCs was increased when the charge transfer resistance was reduced. The highest FF value was 74%, yielded by the two DSSC devices with the lowest charge transfer resistance which were the TiO₂-5% Pb sintered at 250°C and the control DSSC sample sintered at 450°C, as discussed in the EIS analysis.

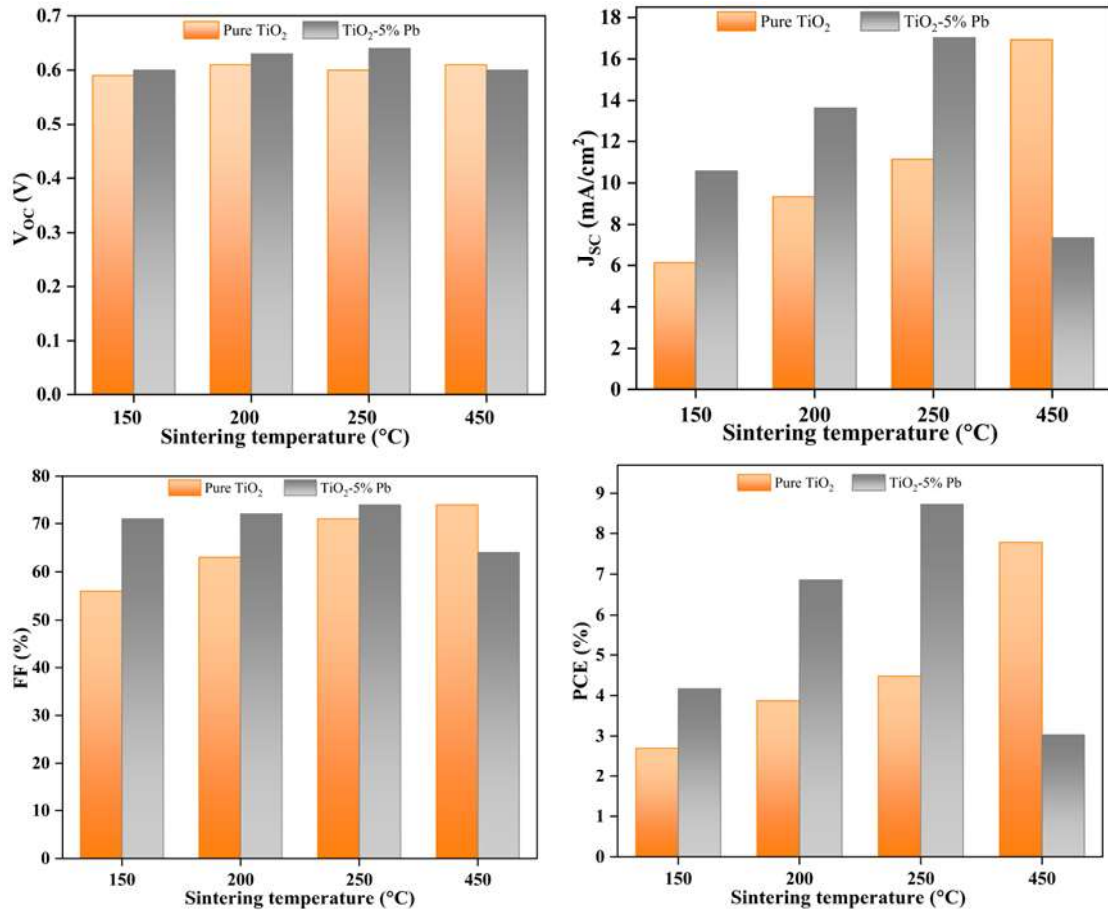


Figure 8: V_{OC} , J_{SC} , FF and PCE at different sintering temperatures

Considering the aforementioned parameters' results, the power conversion efficiency (PCE) of DSSCs have also been determined. As the V_{OC} , J_{SC} , and FF values increased, the PCE value also been increased. The highest PCE value obtained in the research was 8.73% for DSSC based on TiO₂-5% Pb photoanode sintered at 250°C. This value was even higher than control DSSC prepared with pure TiO₂ at high sintering temperature of 450°C with PCE of 7.78%. Hence, highlighting the superiority in performance of the TiO₂-Pb photoanode despite the low sintering temperature. The improved interparticle connection due to the necking at the TiO₂-Pb interface during the liquid phase sintering process have been attributed as the main cause for such good performance. The yielded PCE value have also been supported by the low R_{CT} value obtained in the EIS analysis. With lower R_{CT} , the electrons were easily transferred into the TiO₂ surface, enhancing the DSSC performance. The nanocomposite photoanode have also shown the highest dye loading value of $1.17 \times 10^{-7}/\text{cm}^2$, indicating high light harvesting capability. Besides, DSSC sample based on TiO₂-5% Pb photoanode sintered at high temperature of 450°C has also been prepared for comparison purposes with the low temperature DSSC. The result showed that the PCE value for this sample to be lower at 3.03%. The decrease

1
2
3
4
5
6
7
8
9
10
11
12
13
14
15
16
17
18
19
20
21
22
23
24
25
26
27
28
29
30
31
32
33
34
35
36
37
38
39
40
41
42
43
44
45
46
47
48
49
50
51
52
53
54
55
56
57
58
59
60
61
62
63
64
65

in efficiency could be attributed to the oxidation of Pb in the TiO₂ matrix since the oxidation temperature of Pb is around 450°C-640°C [38]. Apart from that, the high sintering temperature has caused Pb to be completely melted and causing excessive liquid phase formation that lowers the porosity of the photoanode [39]. Thus, lowering the dye absorption capability of the photoanode and eventually lowers the performance of DSSC. Hence, the DSSC based on TiO₂-5% Pb @ 250°C photoanode has the best performance that was even better than the control DSSC device. These results in Figure 8 highlighted the advantage of liquid phase sintering with Pb sintering aid addition method in yielding high performing DSSC even at low sintering temperature.

4.0 Conclusions

The research aims to improve the efficiency of DSSC devices being prepared at relatively low sintering temperature. Metallic Pb particles as sintering aid has been employed to reduce the sintering temperature of TiO₂ based photoanode. Various concentrations of Pb from 0.5-10wt% has been tried at different sintering temperatures to optimise the electro-optical properties. Increase in Pb concentration and temperature leads to improved PCE. This is due to improved interparticle contact due to surface fusion of Pb. DSSC prepared with TiO₂-5% Pb photoanode sintered at 250°C exhibited highest PCE value of 8.73% surpassing even the high temperature DSSC control samples by approximately 12.21% prepared with pure TiO₂ photoanode sintered at 450°C (PCE: 7.78%). The addition of Pb as sintering aid improved the interparticle connection leading to increased in current density and a reduction in recombination reactions. Further increase in concentration of Pb did not improve the PCE which may be correlated with increased impurities in the TiO₂ matrix, which in turn leads to layer cracking and increased charge trapping sites. Besides Pb, other metallic nanoparticles with low melting point should also be researched in the future by using the liquid phase sintering applied in this research. Metal nanoparticles with a lower melting point could produce highly efficient DSSC at lower sintering temperatures that would be suitable for flexible DSSC substrate. The method has shown to be effective for low sintering temperature operation, is a simple process and there is wide availability of metal nanoparticles that are potentially suitable to be used for future research.

Acknowledgment

The authors would like to acknowledge Ministry of Higher Education Malaysia for financial assistance through Fundamental Research Grant Scheme (FRGS) (FRGS/1/2020/STG05/SYUC/02/1)

Declaration-of-interests

The authors declare that they have no known competing financial interests or personal relationships that could have influenced the work reported in this paper.

References

- [1] K. Sharma, V. Sharma, S.S. Sharma, Dye-Sensitized Solar Cells: Fundamentals and Current Status, *Nanoscale Res Lett.* 13 (2018) 381. <https://doi.org/10.1186/s11671-018-2760-6>.
- [2] M.A. Saeed, K. Yoo, H.C. Kang, J.W. Shim, J.J. Lee, Recent developments in dye-sensitized photovoltaic cells under ambient illumination, *Dyes and Pigments.* 194 (2021) 109626. <https://doi.org/10.1016/j.dyepig.2021.109626>.
- [3] C. Wu, K. Wang, M. Batmunkh, A.S.R. Bati, D. Yang, Y. Jiang, Y. Hou, J.G. Shapter, S. Priya, Multifunctional nanostructured materials for next generation photovoltaics, *Nano Energy.* 70 (2020) 104480. <https://doi.org/10.1016/J.NANOEN.2020.104480>.
- [4] M.S. Ahmad, A.K. Pandey, N. Abd Rahim, N. Aslfattahi, Y.K. Mishra, B. Rashid, R. Saidur, 2-D Mxene flakes as potential replacement for both TCO and Pt layers for Dye-Sensitized Solar cell, *Ceram Int.* 47 (2021) 27942–27947. <https://doi.org/10.1016/j.ceramint.2021.06.225>.
- [5] M.S. Ahmad, N.A. Rahim, Syed shahabuddin, S. Mehmood, A.D. Khan, Effect of WS₂ nano-sheets on the catalytic activity of polyaniline nano-rods based counter electrode for dye sensitized solar cell, *Physica E Low Dimens Syst Nanostruct.* 126 (2021) 114466. <https://doi.org/10.1016/j.physe.2020.114466>.
- [6] J.M. Ji, H. Zhou, Y.K. Eom, C.H. Kim, H.K. Kim, 14.2% Efficiency Dye-Sensitized Solar Cells by Co-sensitizing Novel Thieno[3,2-b]indole-Based Organic Dyes with a Promising Porphyrin Sensitizer, *Adv Energy Mater.* 10 (2020) 2000124. <https://doi.org/10.1002/aenm.202000124>.
- [7] A. Yella, H.W. Lee, H.N. Tsao, C. Yi, A.K. Chandiran, M.K. Nazeeruddin, E.W.G. Diau, C.Y. Yeh, S.M. Zakeeruddin, M. Grätzel, Porphyrin-sensitized solar cells with cobalt (II/III)-based redox electrolyte exceed 12 percent efficiency, *Science* (1979). 334 (2011) 629–634. <https://doi.org/10.1126/science.1209688>.
- [8] H. Min, D.Y. Lee, J. Kim, G. Kim, K.S. Lee, J. Kim, M.J. Paik, Y.K. Kim, K.S. Kim, M.G. Kim, T.J. Shin, S. il Seok, Perovskite solar cells with atomically coherent interlayers on SnO₂ electrodes, *Nature* 2021 598:7881. 598 (2021) 444–450. <https://doi.org/10.1038/s41586-021-03964-8>.
- [9] Y. Cui, Y. Xu, H. Yao, P. Bi, L. Hong, J. Zhang, Y. Zu, T. Zhang, J. Qin, J. Ren, Z. Chen, C. He, X. Hao, Z. Wei, J. Hou, Single-Junction Organic Photovoltaic Cell with 19% Efficiency, *Advanced Materials.* 33 (2021) 2102420. <https://doi.org/10.1002/ADMA.202102420>.

- 1
2
3
4
5
6
7
8
9
10
11
12
13
14
15
16
17
18
19
20
21
22
23
24
25
26
27
28
29
30
31
32
33
34
35
36
37
38
39
40
41
42
43
44
45
46
47
48
49
50
51
52
53
54
55
56
57
58
59
60
61
62
63
64
65
- [10] R. Zhu, Z. Zhang, Y. Li, Advanced materials for flexible solar cell applications, *Nanotechnol Rev.* 8 (2019) 452–458. <https://doi.org/10.1515/ntrev-2019-0040>.
 - [11] G. Li, L. Sheng, T. Li, J. Hu, P. Li, K. Wang, Engineering flexible dye-sensitized solar cells for portable electronics, *Solar Energy.* 177 (2019) 80–98. <https://doi.org/10.1016/J.SOLENER.2018.11.017>.
 - [12] N.S. Noorasid, F. Arith, A.N. Mustafa, M.A. Azam, S. Mahalingam, P. Chelvanathan, N. Amin, Current advancement of flexible dye sensitized solar cell: A review, *Optik (Stuttg).* 254 (2022) 168089. <https://doi.org/10.1016/j.ijleo.2021.168089>.
 - [13] J. Zhang, Z. Wang, X. Li, J. Yang, C. Song, Y. Li, J. Cheng, Q. Guan, B. Wang, Flexible Platinum-Free Fiber-Shaped Dye Sensitized Solar Cell with 10.28% Efficiency, *ACS Appl Energy Mater.* 2 (2019) 2870–2877. <https://doi.org/10.1021/acsaem.9b00207>.
 - [14] H. Khir, A.K. Pandey, R. Saidur, M. Shakeel Ahmad, N. Abd Rahim, M. Dewika, M. Samykan, Recent advancements and challenges in flexible low temperature dye sensitised solar cells, *Sustainable Energy Technologies and Assessments.* 53 (2022) 102745. <https://doi.org/10.1016/J.SETA.2022.102745>.
 - [15] M.E. Yeoh, K.Y. Chan, Recent advances in photo-anode for dye-sensitized solar cells: a review, *Int J Energy Res.* 41 (2017) 2446–2467. <https://doi.org/10.1002/er.3764>.
 - [16] S. Ni, F. Guo, D. Wang, S. Jiao, J. Wang, Y. Zhang, B. Wang, P. Feng, L. Zhao, Modification of TiO₂ nanowire arrays with Sn doping as photoanode for highly efficient dye-sensitized solar cells, *Crystals (Basel).* 9 (2019) 113. <https://doi.org/10.3390/cryst9020113>.
 - [17] R.S. Dubey, S.R. Jadkar, A.B. Bhorde, Synthesis and Characterization of Various Doped TiO₂ Nanocrystals for Dye-Sensitized Solar Cells, *ACS Omega.* 6 (2021) 3470–3482. <https://doi.org/10.1021/acsomega.0c01614>.
 - [18] L. Song, J. Zhai, P. Du, J. Xiong, F. Ko, A novel bilayer photoanode made of carbon nanotubes incorporated TiO₂ nanorods and Mg²⁺ doped TiO₂ nanorods for flexible dye-sensitized solar cells, *Thin Solid Films.* 646 (2018) 44–52. <https://doi.org/10.1016/j.tsf.2017.11.030>.
 - [19] R. de Oro Calderon, C. Gierl-Mayer, H. Danninger, Fundamentals of Sintering: Liquid Phase Sintering, *Encyclopedia of Materials: Metals and Alloys.* 3 (2022) 481–492. <https://doi.org/10.1016/B978-0-12-819726-4.00127-7>.
 - [20] M.S. Ahmad, N.A. Rahim, A.K. Pandey, Improved electron transfer of TiO₂ based dye sensitized solar cells using Ge as sintering aid, *Optik (Stuttg).* 157 (2018) 134–140. <https://doi.org/10.1016/j.ijleo.2017.11.073>.
 - [21] M.S. Ahmad, A.K. Pandey, N.A. Rahim, S. Shahabuddin, S.K. Tyagi, Chemical sintering of TiO₂ based photoanode for efficient dye sensitized solar cells using Zn nanoparticles, *Ceram Int.* 44 (2018) 18444–18449. <https://doi.org/10.1016/j.ceramint.2018.07.062>.

- 1
2
3
4
5
6
7
8
9
10
11
12
13
14
15
16
17
18
19
20
21
22
23
24
25
26
27
28
29
30
31
32
33
34
35
36
37
38
39
40
41
42
43
44
45
46
47
48
49
50
51
52
53
54
55
56
57
58
59
60
61
62
63
64
65
- [22] P.S. Liu, G.F. Chen, Making Porous Metals, in: *Porous Materials - Processing and Applications*, Elsevier, 2014: pp. 21–112. <https://doi.org/10.1016/b978-0-12-407788-1.00002-2>.
- [23] A. Mallick, I. Visoly-Fisher, Pb in halide perovskites for photovoltaics: Reasons for optimism, *Mater Adv.* 2 (2021) 6125–6135. <https://doi.org/10.1039/d1ma00355k>.
- [24] R. Long, Y. Dai, G. Meng, B. Huang, Energetic and electronic properties of X- (Si, Ge, Sn, Pb) doped TiO₂ from first-principles, *Physical Chemistry Chemical Physics.* 11 (2009) 8165–8172. <https://doi.org/10.1039/b903298c>.
- [25] H. Khan, Y. Iqbal, M. Khan, S.N. Ahmad, Y. Zeng, Variations in the optical properties of TiO₂ with Pb doping using ab initio calculations, *Int J Mod Phys B.* 35 (2021) 29. <https://doi.org/10.1142/S0217979221502969>.
- [26] A.K. Mishra, S. Saha, FABRICATION AND CHARACTERIZATION OF NATURAL DYE SENSITIZED SOLAR CELLS BASED ON PbS NANOSTRUCTURES, *Chalcogenide Letters.* 17 (2020) 605–614. https://chalcogen.ro/605_MishraAK.pdf (accessed September 7, 2022).
- [27] R. Singh, S.P. Pandey, P.K. Shukla, S.K. Tomar, B. Bhattacharya, P.K. Singh, Synthesis of lead sulphide nanoparticles for electrode application of dye sensitized solar cells, *Nanoscience and Nanotechnology Letters.* 6 (2014) 31–36. <https://doi.org/10.1166/nnl.2014.1722>.
- [28] J. Jia, H. Yamamoto, T. Okajima, Y. Shigesato, On the Crystal Structural Control of Sputtered TiO₂ Thin Films, *Nanoscale Res Lett.* 11 (2016) 324. <https://doi.org/10.1186/s11671-016-1531-5>.
- [29] J. He, Y. en Du, Y. Bai, J. An, X. Cai, Y. Chen, P. Wang, X. Yang, Q. Feng, Facile formation of anatase/rutile TiO₂ nanocomposites with enhanced photocatalytic activity, *Molecules.* 24 (2019) 2996. <https://doi.org/10.3390/molecules24162996>.
- [30] F. Scarpelli, T.F. Mastropietro, T. Poerio, N. Godbert, Mesoporous TiO₂ Thin Films: State of the Art, in: *Titanium Dioxide - Material for a Sustainable Environment*, InTech, 2018: pp. 57–80. <https://doi.org/10.5772/intechopen.74244>.
- [31] Q. Zhang, C. Li, High temperature stable anatase phase titanium dioxide films synthesized by mist chemical vapor deposition, *Nanomaterials.* 10 (2020) 911. <https://doi.org/10.3390/nano10050911>.
- [32] F. Gontad, A. Lorusso, A. Klini, A. Loufardaki, M. Panareo, C. Fotakis, A. Perrone, Picosecond and subpicosecond pulsed laser deposition of Pb thin films, *Physical Review Special Topics - Accelerators and Beams.* 16 (2013). <https://doi.org/10.1103/PhysRevSTAB.16.093401>.
- [33] G.A. Alamu, O. Adedokun, I.T. Bello, Y.K. Sanusi, Plasmonic enhancement of visible light absorption in Ag-TiO₂ based dye-sensitized solar cells, *Chemical Physics Impact.* 3 (2021) 100037. <https://doi.org/10.1016/J.CHPHI.2021.100037>.
- [34] P. Pandey, M.R. Parra, F.Z. Haque, R. Kurchania, Effects of annealing temperature optimization on the efficiency of ZnO nanoparticles photoanode based dye sensitized

1 solar cells, *Journal of Materials Science: Materials in Electronics*. 28 (2017) 1537–
2 1545. <https://doi.org/10.1007/s10854-016-5693-9>.

- 3 [35] B. O'Regan, M. Gratzel, A low-cost, high-efficiency solar cell based on dye-sensitized
4 colloidal TiO₂ films, *Nature*. 353 (1991) 737–740.
5 <https://doi.org/https://doi.org/10.1038/353737a0>.
6
7 [36] K.G. Baiju, B. Murali, R. Subba Rao, K. Jayanarayanan, D. Kumaresan, Heat sink
8 assisted elevated temperature sintering process of TiO₂ on polymer substrates for
9 producing high performance flexible dye-sensitized solar cells, *Chemical Engineering
10 and Processing - Process Intensification*. 149 (2020) 107817.
11 <https://doi.org/10.1016/j.cep.2020.107817>.
12
13 [37] S.N.F. Zainudin, H. Abdullah, M. Markom, Electrochemical studies of tin oxide
14 based-dye-sensitized solar cells (DSSC): a review, *Journal of Materials Science:
15 Materials in Electronics*. 30 (2019) 5342–5356. [https://doi.org/10.1007/s10854-019-
16 00929-6](https://doi.org/10.1007/s10854-019-00929-6).
17
18 [38] T.E. Weyand, The oxidation kinetics of liquid lead and lead alloys, DOCTORAL
19 DISSERTATIONS, University of Missouri, 1970.
20 https://scholarsmine.mst.edu/doctoral_dissertations/2042.
21
22 [39] A. Sabahi Namini, M. Azadbeh, A. Mohammadzadeh, Microstructure and
23 densification behavior of liquid phase sintered Cu-28Zn prealloyed powder, *Science of
24 Sintering*. 45 (2013) 351–362. <https://doi.org/10.2298/SOS1303351S>.
25
26
27
28
29
30
31
32
33
34
35
36
37
38
39
40
41
42
43
44
45
46
47
48
49
50
51
52
53
54
55
56
57
58
59
60
61
62
63
64
65

Improved charge transfer through the minimal addition of Pb as a sintering aid to TiO₂-based low-temperature dye sensitised solar cell

Hazim Khir^a, A. K. Pandey^{a,b*}, R. Saidur^{a,f}, Muhammad Shakeel Ahmad^c, Nasrudin Abd Rahim^c, M. Dewika^d, M. Samykan^e

^aResearch Centre for Nanomaterials and Energy Technology (RCNMET), School of Engineering & Technology, Sunway University, No. 5, Jalan Universiti, Bandar Sunway, Petaling Jaya, 47500 Selangor Darul Ehsan, Malaysia

^bSunway Materials Smart Science and Engineering (SMS2E) Research Cluster, Sunway University, No. 5 Jalan Universiti, Bandar Sunway, Petaling Jaya 47500, Selangor, Malaysia

^cHigher Institution Centre of Excellence (HiCoE), UM Power Energy Dedicated Advanced Centre (UMPEDAC), Level 4, Wisma R&D, University of Malaya, Jalan Pantai Baharu, 59990 Kuala Lumpur, Malaysia

^dCentre of American Education, Sunway University, No. 5, Jalan Universiti, Bandar Sunway, Petaling Jaya, 47500 Selangor Darul Ehsan, Malaysia

^eCollege of Engineering, University Malaysia Pahang, Lebuhraya Tun Razak, 26300 Gambang, Kuantan, Pahang, Malaysia

^fSchool of Engineering, Lancaster University, LA1 4YW, United Kingdom

Abstract

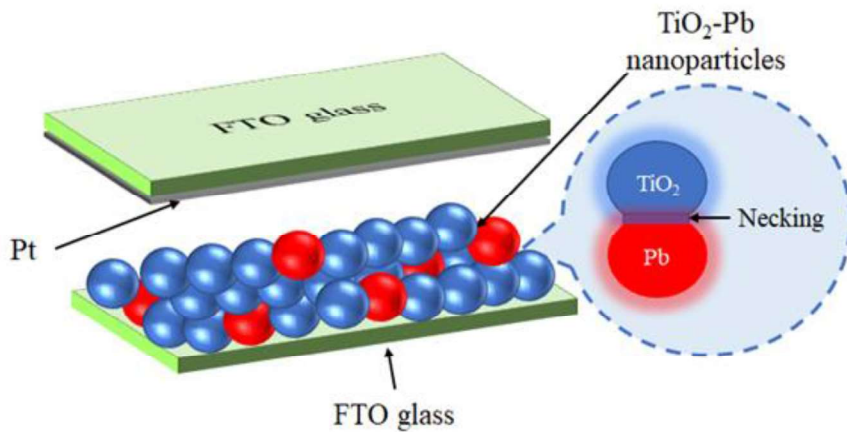
The poor interparticle connectivity between the nanoparticles architecture of photoanode due to ~~the~~ insufficient sintering temperature has been an issue for developing flexible dye sensitised solar cell (DSSC). This issue has led flexible DSSC to yield low conversion efficiency. This research aims to implement lead (Pb) as sintering aid to improve the interparticle connection of the photoanode by using the concept of liquid phase sintering. With low melting point of Pb (327.5°C), necks were formed at the titanium dioxide (TiO₂)-Pb interface that improved the connection and lowered the electronic resistance even at low sintering temperature of 150-250°C. Morphological studies showed the formation of these necks, while phase analysis indicated the more desirable TiO₂ anatase phase was present. Specimens containing 5wt% Pb in the TiO₂ matrix showed the highest efficiency value of 8.73% at 250°C, which is even higher compared to ~~their~~ high-temperature (450°C) counterpart by 12.21%. This is due to surface fusion of Pb at a lower temperature, leading to enhanced ~~inter-partiele~~interparticle contact and reduction in recombination reactions. Further increase in Pb did not improve the conversion efficiency which can be due to high charge trapping sites and layer cracking due to high amounts of Pb in TiO₂ matrix.

Keywords: Flexible DSSC; photoanode; TiO₂; sintering; low temperature

* Corresponding author: Email (s): adarsh.889@gmail.com; adarshp@sunway.edu.my (A. K. Pandey)

1
2
3
4
5
6
7
8
9
10
11
12
13
14
15
16
17
18
19
20
21
22
23
24
25
26
27
28
29
30
31
32
33
34
35
36
37
38
39
40
41
42
43
44
45
46
47
48
49
50
51
52
53
54
55
56
57
58
59
60
61
62
63
64
65

Graphical abstract



Highlights

- Lowered resistance and improved connection due to neck formation between TiO₂-Pb
- Sintering of photoanode at low temperatures (150°C, 200°C and 250°C)
- 12.21% enhancement of DSSC efficiency with Pb sintering aid
- 5wt% Pb in the TiO₂ matrix showed the highest efficiency value of 8.73%

Contents

1.0 Introduction3

2.0 Methodology6

2.1 Materials6

2.2 Preparation of Pb sintering aid6

2.3 Preparation of photoanode samples7

2.4 Fabrication of DSSC devices7

2.5 Characterisation and analysis process8

3.0 Results and discussion9

3.1 Morphological studies9

3.2 Light absorption studies14

3.3 Electron transfer studies17

3.4 I-V curve20

4.0 Conclusions26

References27

1.0 Introduction3

Formatted: Default Paragraph Font, Font: Not Bold, Check spelling and grammar

1
2
3
4
5
6
7
8 The cost of DSSC manufacturing can be decreased by developing flexible DSSC using
9 flexible materials such as plastic substrate made up of indium tin oxide-
10 polyethyleneterephthalate (ITO-PET) and indium tin oxide-polyethylenaphtalate (ITO-PEN).
11 These materials are flexible, lightweight, have good transmittance and conductivity ~~while also~~
12 ~~having with~~ low production cost by utilising roll-to-roll system to mass produce the substrate
13 in ~~the~~ industry [10,11][10,11]. The ability of these materials to be shaped easily allowed them
14 to be applicable for mobile and wearable applications, encouraging ~~the~~ development of flexible
15 DSSC even further [12][12]. Despite all the advantages of the flexible ~~plastic-based~~ DSSCs,
16 these devices suffer from low conversion efficiency compared to rigid glass-based DSSCs with
17 the highest efficiency is reported at 10.28% [13][13].

18
19 A typical rigid glass-based DSSC underwent sintering at high temperature (usually
20 450°C for TiO₂ ~~nanoparticle~~ photoanode) to improve the interparticle connection between the
21 photoanode nanoparticles, remove organic surfactant in the photoanode paste and enhance the
22 adhesion between the photoanode and substrate [14][14]. However, this approach is not
23 applicable for plastic-based DSSC with low thermal stability as the ITO-PET and ITO-PEN
24 polymer substrate would deform at temperature higher than 150°C [11][11]. Hence, ~~a variety~~
25 ~~of various~~ research has been conducted to enhance the efficiency of DSSC ~~even~~ at low sintering
26 temperature.

27
28 One of the approaches that ~~have~~ been taken to enhance the efficiency of DSSC is doping
29 the photoanode with metallic cations materials by tuning the band structure of the photoanode
30 [15][15]. By adding tin (Sn) as dopant to TiO₂ photoanode, Ni et al. [16][16] managed to
31 develop DSSC with good conversion efficiency of 8.75% compared to DSSC with undoped
32 TiO₂ (7.46%). This was attributed to ~~the Sn dopant~~ that expands the electron mobility and raises
33 the flat band potential, eventually improved the performance of DSSC. Dubey et al. [17][17]
34 meanwhile studied a variety of dopants such as vanadium (V), iron (Fe), chromium (Cr) and
35 cobalt (Co) to TiO₂ photoanode, which produced DSSC with efficiency of 3.33%, 4.85%,
36 3.29% and 3.20% respectively compared to pure TiO₂ (1.31%). Thus, highlighting the
37 effectiveness and potential in using dopants as there are wide availability of materials that can
38 still be studied. Dopants have also shown to be effective for flexible DSSC that was sintered at
39 low temperature of 130°C. ~~This was as demonstrademonstrated~~ by Song et al. [18][18] where
40 magnesium (Mg) was used as doping material to TiO₂ photoanode. An increase in efficiency
41 can be seen as Mg-doped TiO₂ DSSC yielded an efficiency of 2.2% compared to undoped ones
42 (1.7%) due to the change in the conduction band state of TiO₂ surface.

1
2
3
4
5
6
7
8
9
10
11
12
13
14
15
16
17
18
19
20
21
22
23
24
25
26
27
28
29
30
31
By using the surface plasmon resonance effects found in metallic nanoparticles and the concept of liquid phase sintering, another approach can also be taken to improve the DSSC sintering process. Liquid phase sintering utilises at least two chemical elements mixed at different compositions, with the major component remaining as solid while the minor component becomes the aids that forms liquid during sintering [19][19]. Liquid phase sintering enhances the sintering mechanism by enhancing the diffusion speed and mass transfer mechanism. Ahmad et al. [20][20] utilises germanium (Ge) as sintering aid to TiO₂ photoanode, where they discovered necks were formed at the TiO₂-Ge interface during sintering. These necks helped improve the interparticle connection leading to better efficiency from 4.03% for pure TiO₂ photoanode to 5.65% with the addition of Ge sintering aid. In another study, Ahmad et al. [21][21] applied zinc (Zn) nanoparticles as sintering aid to TiO₂ nanoparticles with lower sintering temperature of 200°C. A similar outcome was obtained with necks forming at the TiO₂-Zn inter~~face~~phase, improving the efficiency from 4.27% for pure TiO₂ photoanode sintered at 450°C, to 4.92%. Due to the low melting point of Zn (419.5°C), the necks were formed despite the low sintering temperature because of the rules of metallurgical sintering. In metallurgical sintering, the sintering temperature of metals are typically found at around 67-75% of the metals' melting point [22][22]. Hence, ~~addition of~~sintering aid for liquid phase is suitable for both high and low temperature DSSC development.

32
33
34
35
36
37
38
39
40
41
42
43
44
45
46
47
48
Lead (Pb) ~~has high durability, density and is a highly durable and~~ corrosion resistant metal with a low melting point of 327.5°C [23][23]. Pb is a group IV element similar to Ge and Sn which have shown good photocatalytic activity with ~~TiO₂-TiO₂ which~~ has encouraged some previous studies to try reproduce similar outcomes ~~as the other metals~~. Pb was used as dopant material with TiO₂ that has tuned the energy bandgap and electronic structure of TiO₂, extending the wavelength response for solar light, increasing the number of photogenerated electrons and enhances the photocatalytic activity of Pb-doped TiO₂ films [24,25][24,25]. Lead sulphide (PbS) nanoparticles with their tuneable band gap have been used as photoanode material for DSSC in a study by Mishra & Saha [26][26] with power conversion efficiency (PCE) of 1.92%. PbS has also been used with TiO₂ photoanode to form nanocomposite paste in a study by Singh et al. [27][27] which produced DSSC with efficiency of 0.35%, compared to the pure TiO₂ photoanode (0.08%).

49
50
51
52
53
54
55
56
57
58
59
60
61
62
63
64
65
Overall as can be seen from the above literature review, yet extensive studies have not been conducted using pure Pb metal nanoparticles in DSSC development. Besides, the implementation of metal nanoparticles as sintering aid to DSSC photoanode has still not been

Formatted: Font color: Blue

1
2
3
4
5
6
7 a widely research topic in this field. However, metal type of nanoparticles have great potential
8 to enhance the power conversion efficiency (PCE) of DSSCs especially for low temperature
9 applications. Thus, this research aims to develop highly efficient DSSC at low sintering
10 temperature with novel implementation of Pb as sintering aid to TiO₂ photoanode. The low
11 melting point and high charge carrier mobility would make them a suitable sintering aid to
12 form necks with the TiO₂ nanoparticles despite the low sintering temperature [23]. Several
13 different compositions of Pb and low sintering temperatures will also be are investigated to
14 study their effects on the performance of DSSC as well as determining the optimal condition.
15 Highest PCE (8.73%) is found to be for specimens containing 5wt% Pb in the TiO₂ matrix at
16 250°C which outperform as compared to their high-temperature (450°C) counterpart (having
17 PCE of 7.78%) by 12.21%. Besides, the low cost of Pb due to the abundance of the material
18 is another key factor in supporting the viability of this novel research to develop low cost DSSC
19 with good efficiency. Thus, this research aims to apply Pb nanoparticles as a sintering aid to
20 TiO₂ photoanode to develop highly efficiency DSSC even at low sintering temperature. The
21 low melting point of Pb would make them a potentially suitable sintering aid even at low
22 sintering temperature to form necks with TiO₂ nanoparticles and eventually improve the
23 efficiency of DSSC. Several different sintering temperatures as well as varying composition of
24 Pb will be investigated in this study to study their effects on the overall performance of DSSC.
25
26
27
28
29
30
31
32

33 **2.0 Methodology**

34 **2.1 Materials**

35
36 Titania (TiO₂) paste (Sigma-Aldrich), fluorine tin oxide (FTO) glass (Sigma-Aldrich,
37 surface resistivity: 13Ω/sq), Pb powder (Sigma-Aldrich, 100 mesh), platinum (Pt)-coated FTO
38 glass (Solaronix), iodolyte An-50 (Solaronix), ruthenizer 535-bisTBA (Solaronix), methanol
39 (Fisher Scientific), acetonitrile (Fisher Scientific), ethanol (Fisher Scientific), binder clips.
40
41

42 **2.2 Preparation of Pb sintering aid**

43
44 20g of Pb powder (100 mesh) was deposited into a grinding bowl with zirconia balls
45 for the grinding process using a planetary ball mill (Fritsch Pulverisette 5) operated ~~ran~~ at 500
46 rpm (Fritsch Pulverisette 5). Multiple grinding cycles were conducted until the Pb powder was
47 found to be in nanoparticle size of around 450-500 nm, checked by using a particle size analyser
48 (Anton Paar Lifesizer 500). ~~Energy dispersive X ray (EDX)(EDX model: Oxford Instrument,~~
49 ~~X Max65T) was also used for elemental composition analysis to make sure the grinded samples~~
50 ~~were not contaminated.~~
51
52
53
54
55
56
57
58
59
60
61
62
63
64
65

1
2
3
4
5
6
7 **2.3 Preparation of photoanode samples**

8 Pure FTO glass was cleaned using methanol each time before they were deposited with
9 photoanode materials. A coating area of 1cm x 1cm was prepared by taping up some parts of
10 the FTO glass using cellophane tape. Pure TiO₂ photoanode samples were prepared by
11 depositing some TiO₂ paste onto the coating area and was coated via doctor blade method. The
12 coated sample was left to dry for 1 hour before the tape was removed, leaving a smooth coated
13 surface. The coated FTO glass was then placed onto a hotplate (IKA RCT basic) and was heated
14 at several different temperature (150°C, 200°C, 250°C and 450°C) for 3 hours. After the
15 sintering process, the samples were then kept and secured for the next steps.
16
17

18
19 In order to prepare the Pb-TiO₂ photoanode samples, different amount of grinded Pb
20 powder was added to the TiO₂ paste and mixed to form different weight composition of Pb
21 (0.5wt%, 1wt%, 3wt%, 5wt% and 10wt%). Similar to the previous step, the doctor blade
22 method was used to coat the composite paste onto the FTO glass to form a coating areawith of
23 1cm x 1cm dimensions. The samples were then heated at different temperatures (150°C, 200°C
24 and 250°C) for 3 hours. The sintered photoanode samples were then kept and secured for
25 further use.
26
27
28
29

30 **2.4 Fabrication of DSSC devices**

31 Ruthenium-based dye solution was prepared by dissolving 10mg of ruthenizer powder
32 into 5ml of acetonitrile solution. The photoanode sample was soaked into the dye solution and
33 left inside for 1 day. After 24 hours, the photoanode sample was taken out from the dye solution
34 and was left to dry at room temperature for 5 hours. Pt-coated FTO glass was then combined
35 together with the dyed photoanode sample. A drop of electrolyte was deposited into ento-the
36 sample via a small hole on the Pt-coated FTO glass to complete the device. Binder clips were
37 then used to clip the two components together. Similar process was repeated for all the
38 photoanode samples and the devices were then kept for further use. The schematic diagram for
39 the preparation of photoanode samples and DSSC devices was shown in Figure 1.
40
41
42
43
44
45
46
47
48
49
50
51
52
53
54
55
56
57
58
59
60
61
62
63
64
65

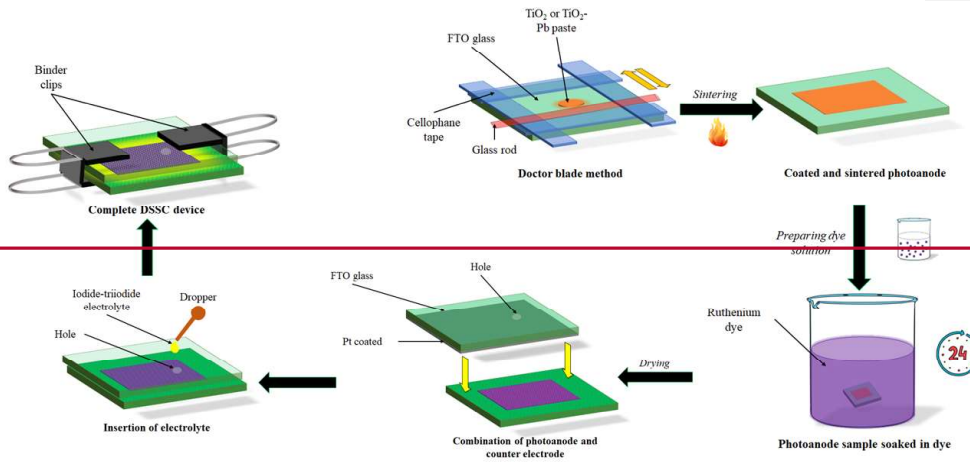


Figure 1: Schematic diagram of the preparation of photoanode samples and fabrication of DSSC devices

2.5 Characterisation and analysis process

Several characterisation studies were conducted on the photoanode samples using equipment such as the field emission scanning electron microscope (FESEM model: Hitachi SU8010) and transmission electron microscope (TEM model: FEI Tecnai G2 20 S-TWIN) for morphological studies. Elemental composition and mapping of the photoanode samples were also investigated using the scanning electron microscope-energy dispersive x-ray (SEM-EDX model: TESCAN VEGA 3) analysis. Phase analysis was also conducted using x-ray diffraction (XRD) analysis (XRD model: Rigaku Miniflex 600). Light absorption studies were also conducted using UV-visible spectroscopy (UV-vis model: PerkinElmer Lambda 750). Electrochemical impedance spectroscopy (EIS) analysis was also conducted using Gamry Interface 1010E Potentiostat to plot the Nyquist and Bode plot. Nyquist plot was used to check for the series (R_s) and charge transfer resistance (R_{CT}) while the Bode plot was applied to determine the electron lifetime (τ) of the DSSC devices. The frequency range was set at 0.1 Hz – 1 MHz and the voltage were set at 10 mV for all samples. Solar simulator (solar simulator model: IVT 300) was also used (~~solar simulator model: IVT 300~~) to measure the current-voltage (I-V) curves, short circuit current (J_{SC}), open circuit voltage (V_{OC}), fill factor (FF) and incident photopower conversion efficiency (IPCEPCE). A 1600W Xenon lamp (SAN-EI electric Co., Ltd) was used in The-IVT 300 series solar simulator uses a 1600W Xenon lamp (SAN-EI electric Co., Ltd). The calibration was done before testing using A_a certified golden

Formatted: Font color: Red

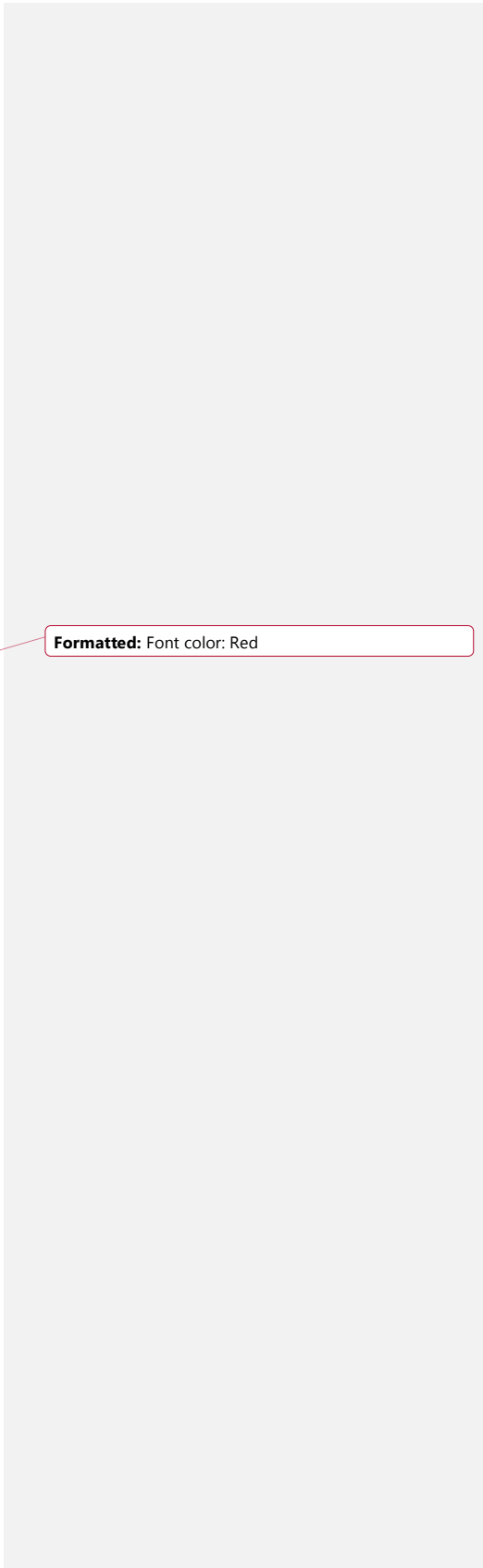
1
2
3
4
5
6
7
8
9
10
11
12
13
14
15
16
17
18
19
20
21
22
23
24
25
26
27
28
29
30
31
32
33
34
35
36
37
38
39
40
41
42
43
44
45
46
47
48
49
50
51
52
53
54
55
56
57
58
59
60
61
62
63
64
65

solar cell (Amorphous Silicon solar cell) ~~has been used to calibrate the machine before testing.~~
The reason behind using Aa standard Amorphous Si solar cell has been selected as it was due to showed minimum mismatch and is assumed to be similar in action spectra with DSSCs. The ealeulated mismatch was found to be approximately 3.7% and, for proper measurements which it was adjusted in machine parameters as a mismatch factor for proper measurements. The data obtained were then analysed and tabulated accordingly in the research. At least 5 samples for each selected sample have been tested and the average value has been presented in this study.

3.0 Results and discussion

3.1 Morphological studies

FESEM equipment have been used to capture the image of the prepared photoanode samples to analyse their morphologies at different sintering temperatures and with the addition of Pb sintering aids. Figure 12 shows the coated and sintered photoanode samples on top of FTO glasses were used for the FESEM analysis ~~and their results as well as the elemental mapping and composition via the SEM-EDX analysis.~~



Formatted: Font color: Red

1
2
3
4
5
6
7
8
9
10
11
12
13
14
15
16
17
18
19
20
21
22
23
24
25
26
27
28
29
30
31
32
33
34
35
36
37
38
39
40
41
42
43
44
45
46
47
48
49
50
51
52
53
54
55
56
57
58
59
60
61
62
63
64
65

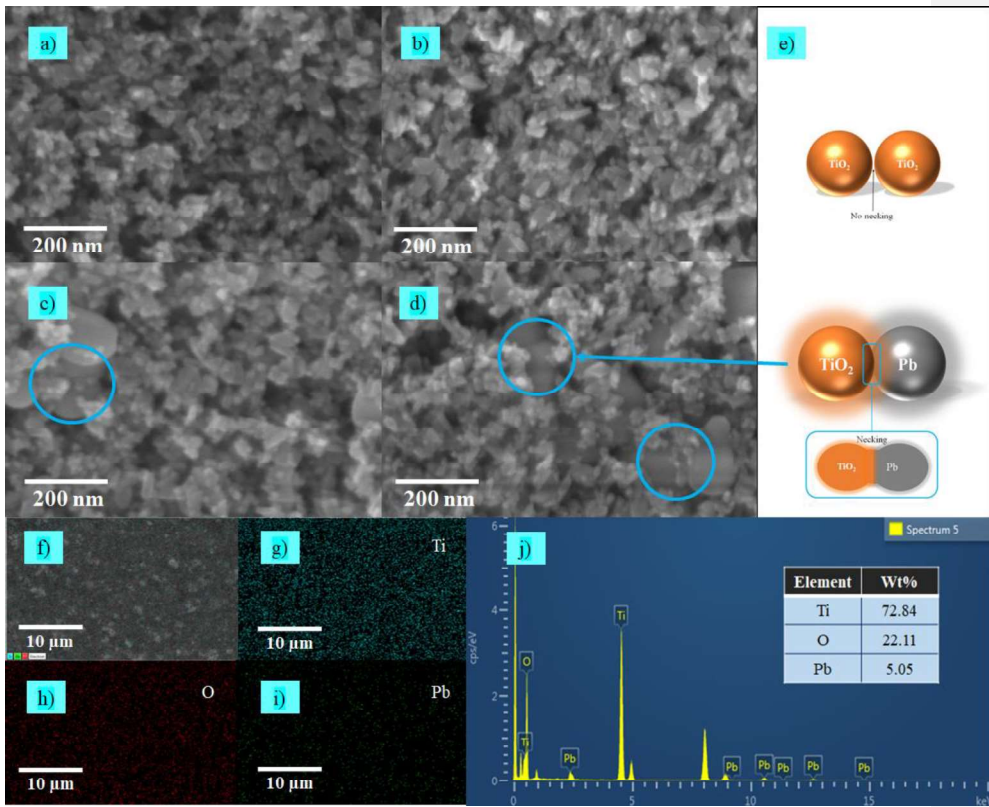
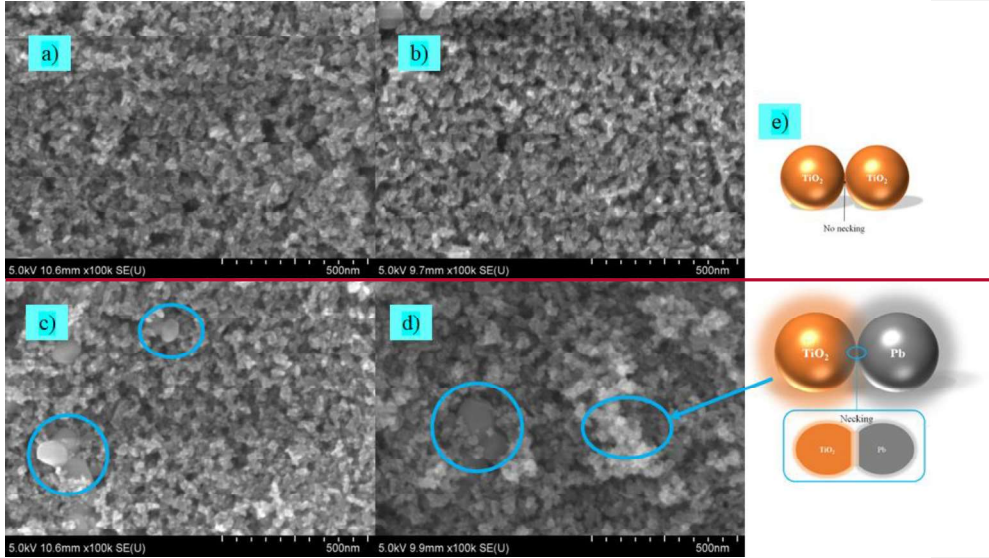


Figure 21: a) FESEM image of pure TiO₂ photoanode sintered at 150°C b) FESEM image of pure TiO₂ photoanode sintered at 250°C c) FESEM image of TiO₂-5% Pb photoanode sintered at 200°C d) FESEM image of TiO₂-5% Pb photoanode sintered at 250°C e) Schematic diagram of the necking between the TiO₂-Pb nanoparticles f)-i) SEM-EDX elemental mapping for Ti, O and Pb elements respectively j) EDX report for TiO₂-5% Pb photoanode sample

FESEM images of the prepared photoanode samples have been depicted in Figure 12a-d. The effect of sintering temperature can be observed from the FESEM images, where the porosity of the films seems to have increased as the sintering temperature increased. The TiO₂ nanoparticles in Figure 12b have also agglomerated more with a denser arrangement than the nanoparticles in Figure 12a due to the increase in sintering temperature. Thus the increase in sintering temperature has enlarged the surface area for better dye absorption, light harvesting and eventually DSSC performance.

Meanwhile, Figures 12c and 12d highlight the presence of Pb sintering aids in the photoanode films. The TiO₂ nanoparticles in both figures have shown better connectivity due to the presence of Pb sintering aid as indicated in the figure. The cause for this improved connection can be attributed to the aforementioned liquid phase sintering and metallurgical sintering theory. Pb nanoparticles have been melted during the sintering process due to their low melting point of 327.5°C. Since the sintering temperature of metal nanoparticles is typically around 70% of their melting point, Pb nanoparticles were sintered well at 250°C [22][22]. The melting of Pb nanoparticles then caused the formation of necks at the TiO₂-Pb interface as shown in Figure 12e, which would enhance the interparticle connectivity of the photoanode. The presence of Pb nanoparticles with the desired elemental composition was also observed in the EDX report of the TiO₂-5% Pb photoanode sample. Elemental mapping for the aforementioned photoanode sample has also been conducted showing the presence of all the elements required in the formation of necks at the TiO₂-Pb interface. The absence of other elements in the EDX analysis indicates that there were no traces of impurities in the prepared photoanode samples. Hence, highlighting the preparation of photoanode samples have been prepared accordingly in the research.

Formatted: Font color: Blue

Formatted: Font color: Blue

Formatted: Font color: Red

Formatted: Font color: Red

Formatted: Font color: Red

Formatted: Font color: Red

Besides FESEM analysis, TEM analysis was also conducted and their images were also observed to study the morphologies of the photoanode samples prepared as shown in Figure 32.

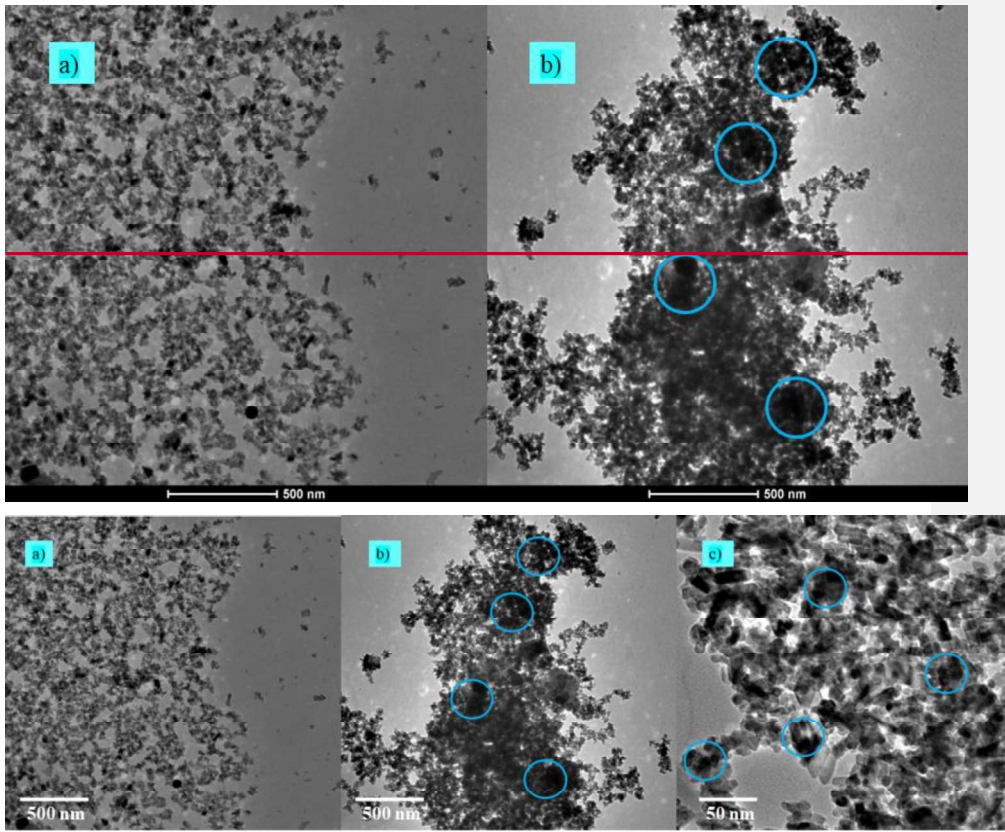


Figure 23: TEM images of photoanode samples a) pure TiO₂ sintered at 250°C b) TiO₂-5% Pb sintered at 250°C with lower magnification c) TiO₂-5% Pb sintered at 250°C with higher magnification

Figure 23 showed the TEM images of photoanode samples prepared at 250°C with and without the addition of Pb sintering aid. The effect of the implementation of Pb sintering aid can clearly be seen in Figure 23b & 2c where there has been an increase in the aggregation between the nanoparticles with the formation of larger chunks of nanoparticles. The highlighted section in Figure 23b & 2c indicates the formation of necks between the TiO₂-Pb nanoparticles during the sintering process. The presence of these nanoparticle aggregations in the TEM images

Formatted: Font color: Red

Formatted: Font color: Red

Formatted: Font color: Red

Formatted: Font color: Red

Formatted: Font color: Red

Formatted: Font color: Red

further supports the observation made in the FESEM images regarding the formation of necks that improve the interparticle connection.

Phase identification of photoanode samples has been conducted via the XRD analysis as shown in Figure 43.

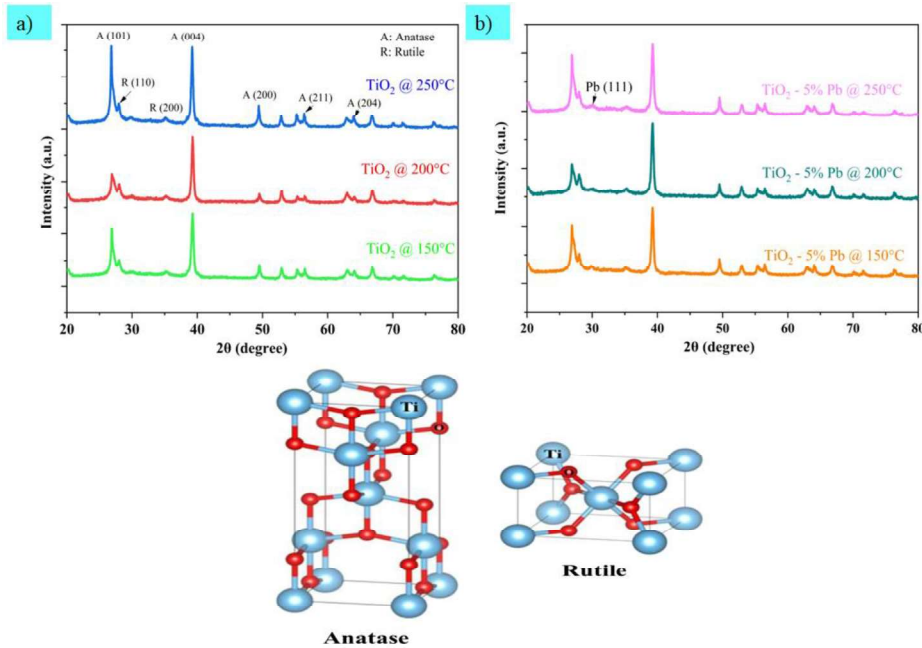


Figure 34: a) XRD analysis of pure TiO₂ photoanode samples at multiple sintering temperature b) XRD analysis of TiO₂ - 5%Pb photoanode samples at multiple sintering temperature with unit cells of anatase TiO₂ and rutile TiO₂ [28][28]

Figure 34a indicates that the peaks have been formed at similar areas for each photoanode sample even with different sintering temperatures. This observation indicates shows that the crystallite structure of TiO₂ did not experience any phase change despite the different sintering temperatures. The more desirable TiO₂ anatase phase have been found to be more prevalent than the less desirable rutile phase as indicated-highlighted in the peaks shown in Figure 34a. Peaks were formed at 2θ positions of 26°, 39°, 49°, 56° and 64° with miller indices of (101), (004), (200), (211) and (204) planes, respectively, indicating TiO₂ anatase phase [29][29]. Meanwhile, a few peaks formed at 27° and 36° with miller indices of (110) and (200) planes, respectively which indicated the TiO₂ rutile phase. The unit cells showed that the Ti-Ti distance

1
2
3
4
5
6
7 is longer, while the Ti-O distance is shorter in anatase phase compared to the rutile phase. This
8 structure would then cause a difference in the mass densities and electronic band structures
9 [30][30]. Hence, anatase TiO₂ have larger bandgap, higher surface energy, lower
10 recombination reaction and smaller grain size, for better photocatalytic and photovoltaic
11 activity [29,31][29,31]. These advantages would eventually lead to a higher DSSC efficiency,
12 making TiO₂ anatase phase more favorable. Pb sintering aid has also been found to not have
13 caused a change in the TiO₂ phase. TiO₂ anatase have remained dominant despite adding Pb as
14 indicated by the peaks formed at 32° with miller indices (111) plane as shown in Figure 34b
15 [32][32]. From these observations, it can be deemed that the low sintering temperature of 150-
16 250°C as well as with the addition of Pb nanoparticles as sintering aid were suitable for
17 maintaining good TiO₂ anatase phase.
18
19
20
21
22

23 3.2 Light absorption studies

24 Light absorption studies for the photoanode materials have been conducted by
25 dissolving an appropriate amount of TiO₂, Pb, and TiO₂-5% Pb into ethanol solvent before they
26 were sonicated for 30 minutes. Pure ethanol solution was then used as a reference, and the
27 outcome from the UV-visible spectroscopy was shown in Figure 45. From the UV-vis spectra,
28 the absorbance peak for TiO₂ sample was at the wavelength of 350 nm. This falls under the
29 UV region as shown in Figure 4, typical for TiO₂ nanoparticles [33]. Similar finding was also
30 obtained for the TiO₂-5% Pb sample where the absorbance peak was formed at a wavelength
31 of 340 nm, also falling in the UV region. The presence of Pb particle can also be found in the
32 nanocomposite with the formation of peak at around 270 nm, similar to the Pb sample. Apart
33 from that, it can be seen that there was higher absorbance for the nanocomposite sample as
34 opposed to pure TiO₂ and Pb sample. The addition of Pb nanoparticles was observed to have
35 helped increase the absorbance of TiO₂-5% Pb sample even beyond the UV region. This was
36 proven by the absorbance peak has been formed at the near-infrared region with wavelength of
37 870 nm, similar to the peak formed by the pure Pb nanoparticle as shown in Figure 4. Hence,
38 indicating the impact of adding Pb nanoparticles as sintering aid to add wavelength response
39 in the near-infrared region for the TiO₂-Pb nanocomposite sample. The improvement in the
40 nanocomposite sample to absorb light at both UV and near-infrared region would help boost
41 their light absorption capabilities. This would eventually enhance the conversion efficiency of
42 the solar device and encourage the implementation of Pb as sintering aid.
43
44
45
46
47
48
49
50
51
52
53
54
55
56
57
58
59
60
61
62
63
64
65

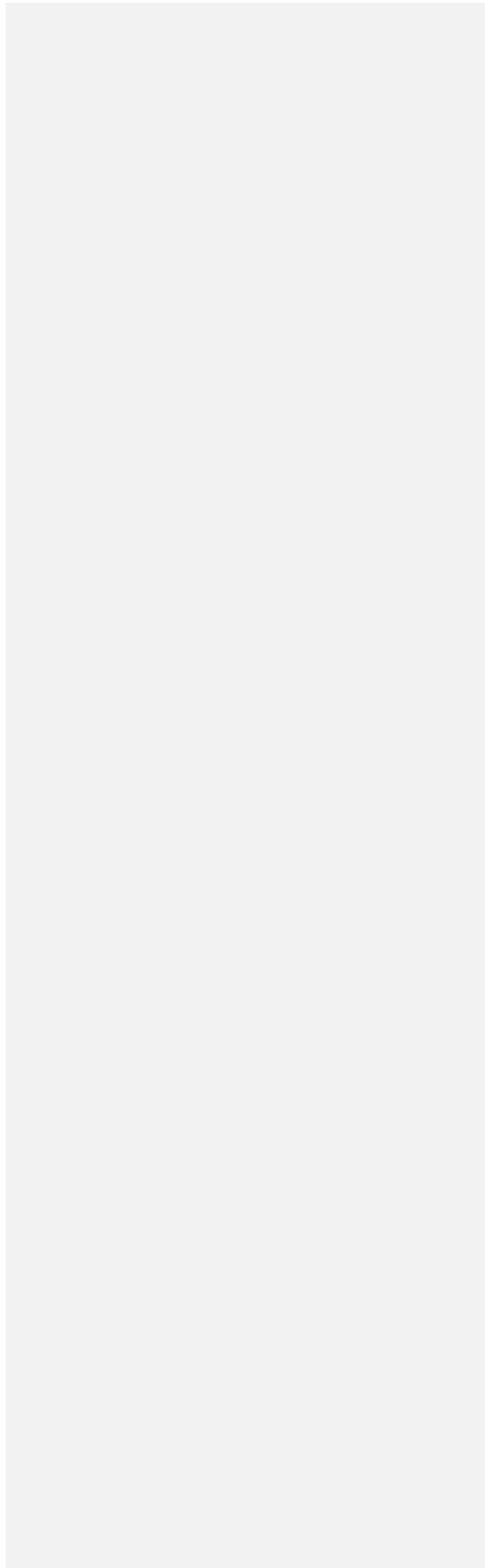
Formatted: Font color: Red

Formatted: Font color: Red

Formatted: Font color: Red

1
2
3
4
5
6
7
8
9
10
11
12
13
14
15
16
17
18
19
20
21
22
23
24
25
26
27
28
29
30
31
32
33
34
35
36
37
38
39
40
41
42
43
44
45
46
47
48
49
50
51
52
53
54
55
56
57
58
59
60
61
62
63
64
65

From the UV-vis spectra, the absorbance peaks for both TiO_2 and TiO_2 -5% Pb was found to have been formed at wavelength of 280 nm. This falls under the UV region as shown in Figure 5, typical for TiO_2 nanoparticles. Higher absorbance has been observed for the nanocomposite as opposed to the pure TiO_2 sample. Thus, indicating the role of Pb in enhancing the absorption of the nanocomposite in the visible light range as highlighted in Figure 5.



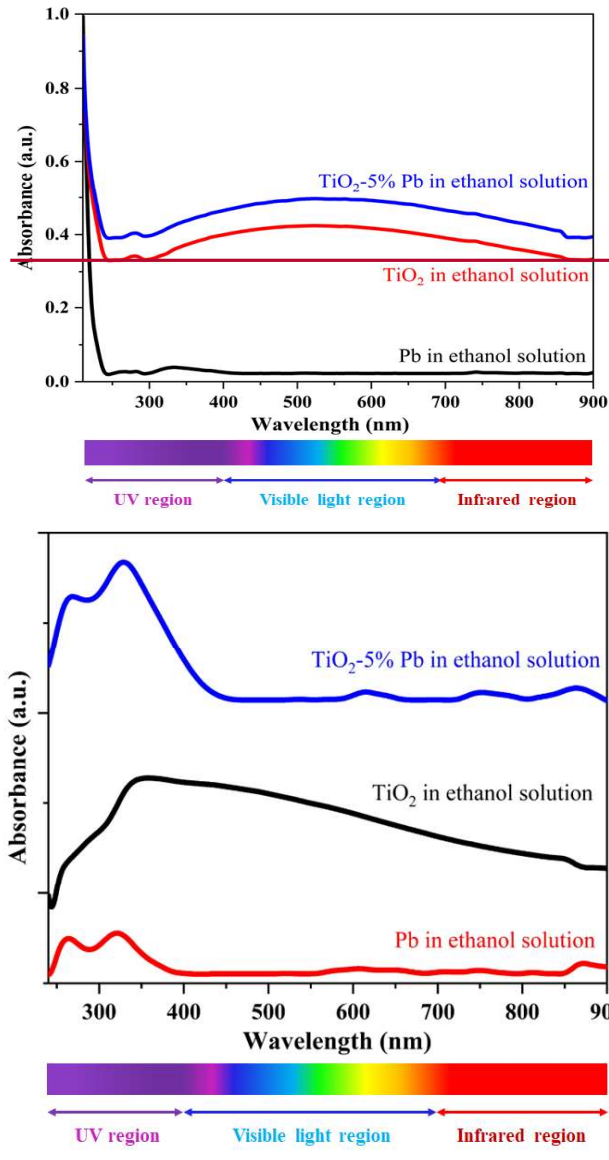


Figure 45: UV-visible spectra of Pb, TiO₂ and TiO₂-5% Pb in ethanol solution.

The difference in the absorbance values between the two samples in the spectra also shows tuning of TiO₂ energy bandgap due to Pb. Therefore, the wavelength response has been

Formatted: Font: 12 pt, Font color: Red

Formatted: Font: 18 pt, Font color: Red

extended towards the visible light region that would improve the photocatalytic activity of the photoanode [25].

3.3 Electron transfer studies

Figure 56 and 67 depicts the Nyquist and Bode plot from EIS analysis which was performed to study the electron transfer of the complete DSSC devices.

EIS response for DSSC devices prepared at 250°C sintering temperature for different Pb composition have been studied. In theory, 250°C was determined to be the most suitable sintering temperature that would yield good results by considering the metallurgical sintering concept [22]. The effect of Pb composition was then studied by analysing the EIS response for these DSSC devices.

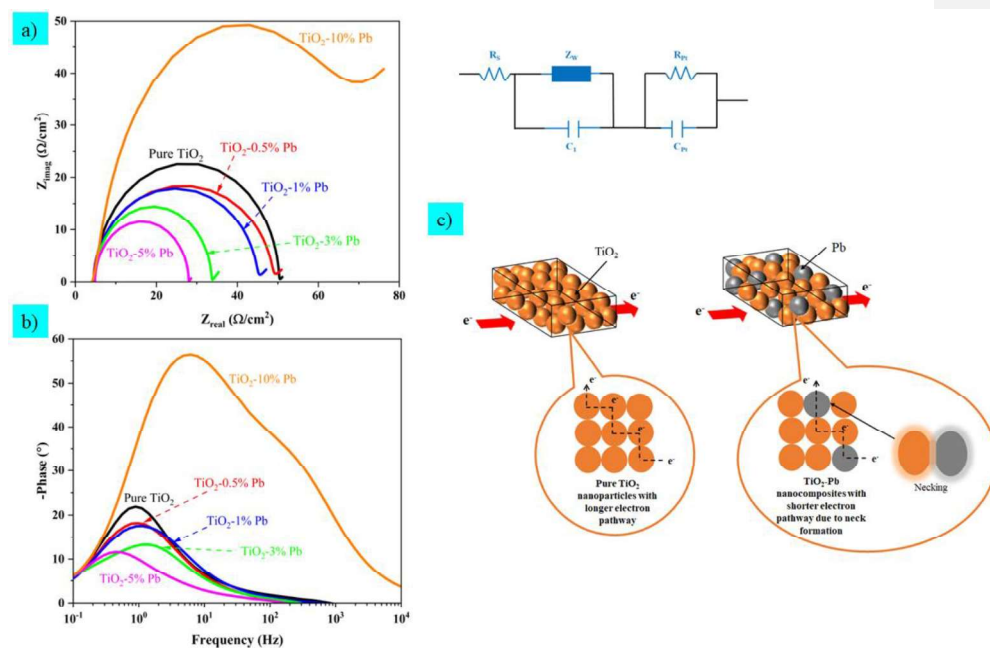


Figure 56: a) Nyquist plot for DSSC devices sintered at 250°C with equivalent circuit b) Bode plot for DSSC devices sintered at 250°C c) Schematic diagram of electron pathway between pure TiO₂ photoanode samples and TiO₂-Pb composite photoanode sample

From the Nyquist plot, the charge transfer resistance (R_{CT}) of DSSC devices was observed to have decreased as Pb sintering aid was implemented to TiO₂ photoanode. The R_{CT} for DSSC

Formatted: Caption, Centered, Don't add space between paragraphs of the same style, Line spacing: 1.5 lines

1
2
3
4
5
6
7 based on pure TiO₂ photoanode was found to be 22.572 Ω/cm², while the R_{CT} for DSSC based
8 on TiO₂-0.5% Pb was 18.317 Ω/cm². The result indicated that the charge transfer capability of
9 the composite photoanode was better. The improvement was attributed to the neck formation
10 between the TiO₂-Pb nanoparticles during the sintering process. The formation of these necks
11 increased the interparticle connectivity from the surface fusion of Pb and the increase in
12 electron density. This occurrence would then led to shorter electron pathway for the transfer of
13 electrons throughout the nanoparticles. With shorter electron pathway, the charge transfer
14 would be improved and the charge transfer properties of the TiO₂-Pb photoanode has been
15 enhanced, eventually reduces the electron pathway throughout the nanoparticles. Thus, the
16 recombination reactions and resistance of DSSC devices have been reduced by adding Pb
17 sintering aid as opposed to pure TiO₂ photoanode with higher resistance values. The R_{CT} was
18 reduced even further as the composition of Pb was increased. The lowest R_{CT} value was
19 discovered when TiO₂-5% Pb photoanode was applied with a value of 11.54 Ω/cm². However,
20 the resistance was found to have increased when the composition of Pb was increased to 10%
21 with high R_{CT} value of 49.29 Ω/cm², higher than pure TiO₂ photoanode. This occurrence was
22 due to excessive amount of Pb, which became impurities that causes electron trapping sites and
23 surface defects [21][24].

24
25
26
27
28
29
30
31 The results from the Nyquist plot were supported even further with the study of Bode
32 plot. From Bode plot, the electron lifetime (*t*) of the DSSC devices was determined using
33 Equation (1) [17][33]:

$$t \text{ (ms)} = \frac{1}{2\pi f_{max}} \quad (1)$$

34
35
36
37 Where, *f_{max}* is the maximum frequency from the Bode plot.

38 The *t* value for DSSC based on pure TiO₂ photoanode was calculated to be 179.229 ms while
39 the *t* value for DSSC based on TiO₂-5% Pb photoanode was calculated to be 358.861 ms. The
40 longer the electron lifetime, the lower the possibility of recombination reactions to occur at the
41 TiO₂ network. With low charge transfer resistance, longer electron lifetime and less
42 possibilities of recombination reaction, TiO₂-5% Pb has been concluded as the most suitable
43 composition for DSSC development. Meanwhile, TiO₂-10% Pb composition was considered
44 unsuitable and worse than pure TiO₂ due to the high R_{CT} and low *t* (25.887 ms), with high
45 recombination reaction probability. Further analysis of DSSC fabricated using the TiO₂-5% Pb
46 composition was then conducted to study the effect of sintering temperature.
47
48
49
50
51
52
53
54
55
56
57
58
59
60
61
62
63
64
65

Formatted: Font color: Blue

Formatted: Font color: Blue

Formatted: Font color: Blue

Formatted: Font color: Blue

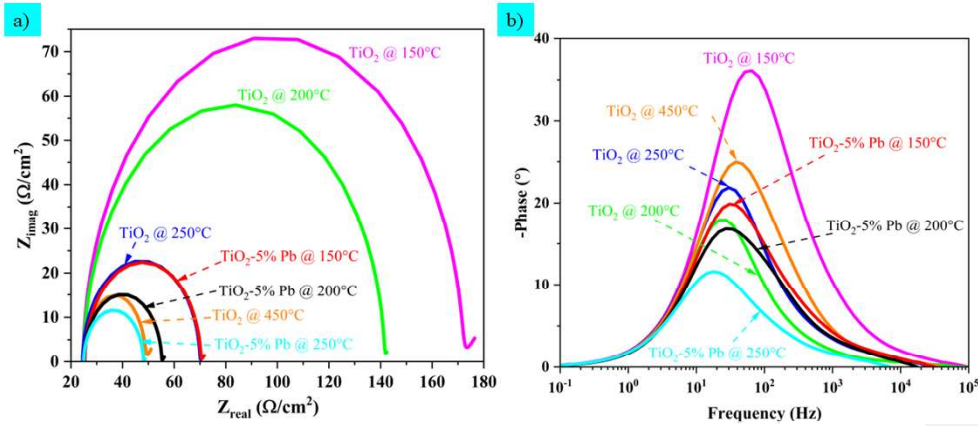
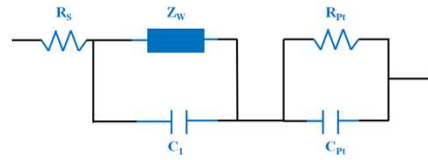


Figure 67: a) Nyquist plot for various DSSC devices with equivalent circuit b) Bode plot for various DSSC devices

EIS analysis for DSSC devices based on TiO₂-5% Pb composition at different sintering temperature was conducted and compared with pure TiO₂ DSSC devices. Figure 67a showed that R_{CT} values decreased as the sintering temperature increases. The highest R_{CT} value was found for DSSC based on pure TiO₂ sintered at 150°C with a value of 72.966 Ω/cm². The photoanode's smaller porosity and surface area lowered the electrical contact between nanoparticles with low and electron transfer that and increased the resistance and recombination reaction [34][34]. To prevent such issue, TiO₂ photoanode is typically sintered at 450°C [35][35]. As shown in Figure 6a, the pure TiO₂ photoanode sintered at 450°C yielded lower R_{CT} value of 14.883 Ω/cm², highlighting the importance of having high sintering temperature. However, in this research, the photoanode samples with Pb addition were sintered at low temperature of 150°C-250°C to be applicable for flexible DSSC development [36].

~~TiO₂ photoanode is sintered at 250°C for flexible DSSC applications.~~

Additionally, the absence of sintering aid also hindered the connection between the TiO₂ nanoparticles. Lower R_{CT} values (22.418 Ω/cm²) was obtained when 5% Pb was added, even at 150°C sintering temperature. The lowest R_{CT} value of 11.54 Ω/cm² was obtained when TiO₂-5% Pb photoanode sintered at 250°C was implemented. The value was even lower than

1
2
3
4
5
6
7 the ~~typical control~~ DSSC based on TiO₂ photoanode sintered at 450°C ($R_{CT} = 14.883 \Omega/\text{cm}^2$).
8
9 Due to the concept of liquid phase and metallurgical sintering, Pb, with a melting point of
10 327.5°C, has melted and formed necks at the TiO₂-Pb interface [19][49]. The interparticle
11 connection of the photoanode have been greatly enhanced, while the charge transfer resistance
12 and recombination reactions have been lowered. Besides the Nyquist plot, Bode plot have also
13 been analysed to calculate the electron lifetime of DSSC. The longest electron lifetime value
14 was obtained for DSSC based on TiO₂-5% Pb photoanode sintered at 250°C with a value of
15 358.861 ms. Thus, lowering the recombination reactions of the DSSC and lowering the
16 resistance as previously mentioned. From the EIS analysis, DSSC based on TiO₂-5% Pb
17 photoanode sintered at 250°C has demonstrated the potential to have the best performance.
18
19
20
21

22 3.4 I-V curve

23 The current-voltage (I-V) characteristics of the prepared DSSC devices have been
24 determined using a solar simulator and was plotted in Figure 78. From the solar cell I-V curve,
25 several important parameters in evaluating the performance of DSSC have also been calculated
26 and tabulated in Table 1 along with dye loading. Dye loading for the DSSC was also performed
27 via the absorption-desorption method was performed, and sodium hydroxide (NaOH)-ethanol
28 solution was used to desorb the dye loaded on the photoanode samples. The outcome of the
29 dye loading was also presented in Table 1. Control DSSC _device prepared with pure TiO₂
30
31
32
33
34
35
36
37
38
39
40
41
42
43
44
45
46
47
48
49
50
51
52
53
54
55
56
57
58
59
60
61
62
63
64
65

photoanode sintered at 450°C was used as reference, thus, comparisons can be made between the prepared ~~DSSC~~ and control typical DSSC.

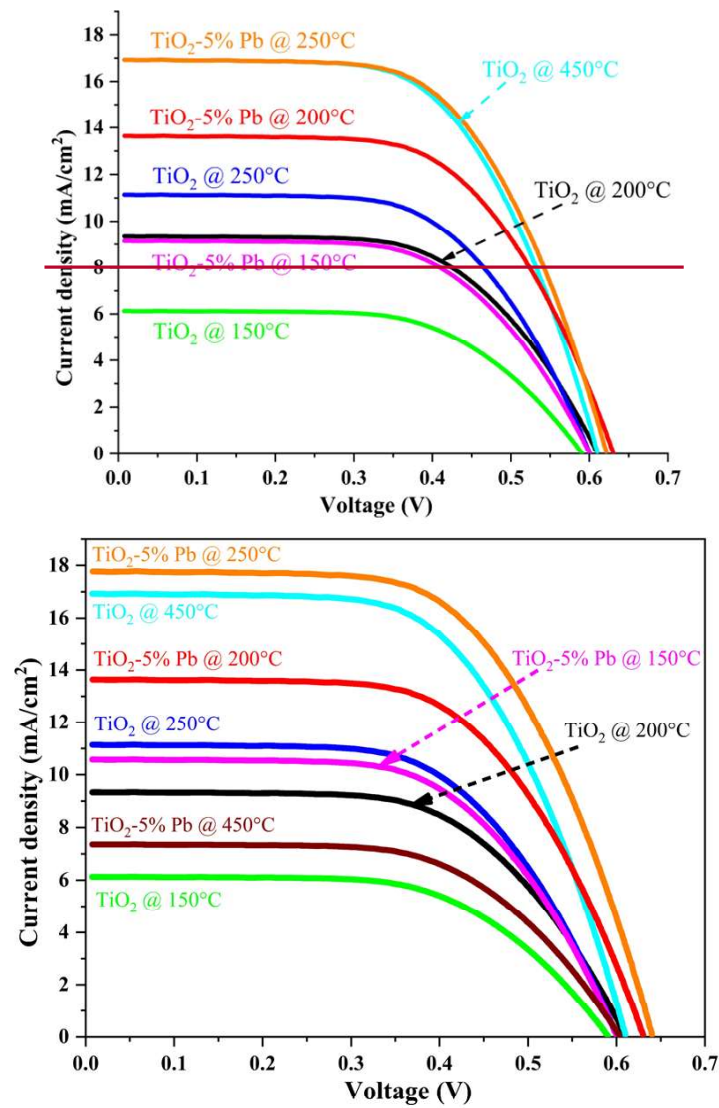


Figure 78: I-V curve for the prepared DSSC devices

Increased sintering temperature burned out more organic compounds and impurities in TiO₂ nanoparticles, which led to an enlarged surface area [34][34]. This then improved their dye

Formatted: Font color: Accent 2

Formatted: Font: Not Italic

loading capability, eventually enhancing their light harvesting capability. Meanwhile, improvement in the interparticle connection between the TiO₂ nanoparticles from the addition of Pb sintering aid have also shown to have improved the dye loading ability of the photoanode samples. The highest dye loading was obtained for the TiO₂-5% Pb photoanode sample sintered at 250°C with a value of 1.17 x 10⁻⁷/cm². ~~This was higher than the typical control DSSC sample pure TiO₂ photoanode sintered at high temperature of 450°C.~~ Thus, indicating that the prepared nanocomposite photoanode have good dye loading and light absorption capability that would eventually enhance the DSSC performance.

Table 1: Summary of parameters of DSSC samples

| Photoanode sample | Sintering temperature (°C) | IPCE/PCE (%) | V _{oc} (V) | J _{sc} (mA/cm ²) | FF (%) | Dye loading (× 10 ⁻⁷ /cm ²) |
|------------------------------|----------------------------|--------------|---------------------|---------------------------------------|-----------|--|
| TiO ₂ | 150 | 2.70 | 0.59 | 6.13 | 56 | 1.01 |
| TiO ₂ | 200 | 3.87 | 0.61 | 9.34 | 63 | 1.03 |
| TiO ₂ | 250 | 4.48 | 0.60 | 11.14 | 71 | 1.03 |
| TiO ₂ | 450 | 7.78 | 0.61 | 16.93 | 74 | 1.06 |
| TiO ₂ - 5% Pb | 150 | 4.17 | 0.60 | 9.14 10.58 | 71 | 1.02 |
| TiO ₂ - 5% Pb | 200 | 6.86 | 0.63 | 13.64 | 72 | 1.08 |
| TiO ₂ - 5% Pb | 250 | 8.73 | 0.64 2 | 17.78 6.93 | 74 | 1.17 |
| <u>TiO₂-5% Pb</u> | <u>450</u> | <u>3.03</u> | <u>0.60</u> | <u>7.36</u> | <u>64</u> | <u>n/a</u> |

Table 1 shows that the open circuit voltage (V_{oc}) values for the samples underwent minimal changes and were slightly increased when Pb was added as a sintering aid. The values

Formatted: Indent: First line: 0"

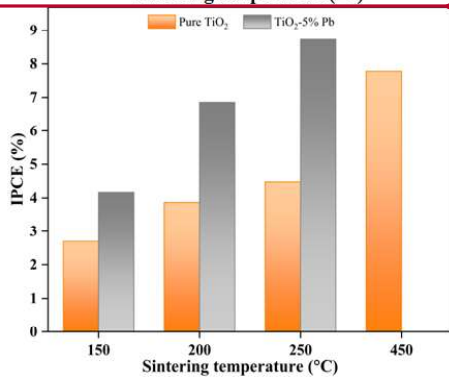
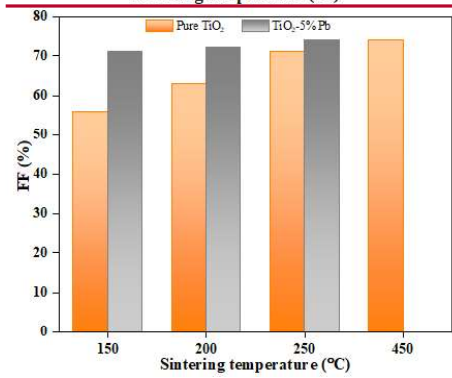
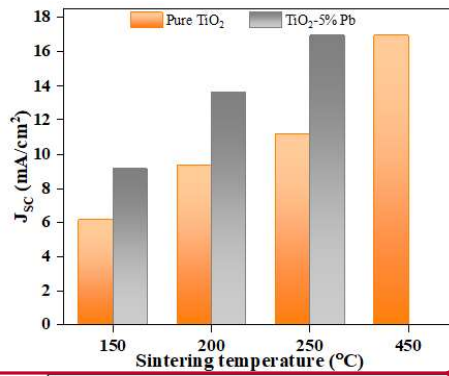
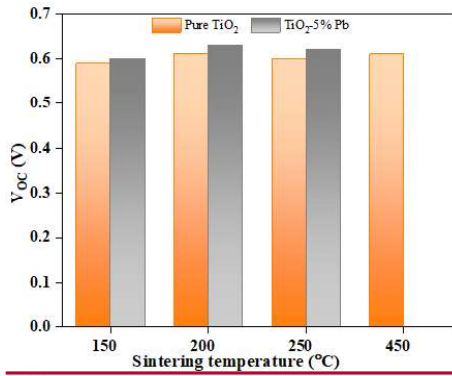
Formatted: Font color: Accent 2

Formatted: Font color: Accent 2

1
2
3
4
5
6
7 of V_{OC} depend on the difference between the Fermi energy level of photoanode and
8 electrolyte's redox potential [37][36]. ~~With the addition of Pb nanoparticles, the conduction~~
9 ~~band shifted to higher energy and increased the V_{OC} values.~~ The short circuit current (J_{SC}) was
10 discovered to have improved when the sintering temperature was increased and Pb sintering
11 aid was added. The increased J_{SC} can be attributed to the enhanced dye absorption with higher
12 charge transfer and lower recombination in the photoanode [15,37][15,36]. The increased
13 ~~interparticle contact, interconnected~~ porosity and enlarged surface area from the increase in
14 sintering temperature, have caused these changes, with ~~the highest~~ high J_{SC} value of 16.93
15 mA/cm² obtained for DSSC sintered at 450°C.
16
17
18
19

20 Meanwhile, the lowest J_{SC} (6.13 mA/cm²) was yielded by DSSC photoanode sintered
21 at a low temperature of 150°C with a small surface area and low dye absorption. DSSC based
22 on TiO₂-5% Pb photoanode sintered at a lower temperature of 250°C has also yielded the
23 highest J_{SC} value. Thus, indicating that the presence of Pb nanoparticles has also improved the
24 interparticle connectivity, dye absorption, and charge transfer. The recombination reaction has
25 also been lowered as discussed in the EIS analysis. The fill factor (FF) of DSSCs was increased
26 when the charge transfer resistance was reduced. The highest FF value was 74%, yielded by
27 the two DSSC devices with the lowest charge transfer resistance which were the TiO₂-5% Pb
28 sintered at 250°C and the control DSSC sample sintered at 450°C, as discussed in the EIS
29 analysis.
30
31
32
33
34
35
36
37
38
39
40
41
42
43
44
45
46
47
48
49
50
51
52
53
54
55
56
57
58
59
60
61
62
63
64
65

1
2
3
4
5
6
7
8
9
10
11
12
13
14
15
16
17
18
19
20
21
22
23
24
25
26
27
28
29
30
31
32
33
34
35
36
37
38
39
40
41
42
43
44
45
46
47
48
49
50
51
52
53
54
55
56
57
58
59
60
61
62
63
64
65



Formatted: Centered

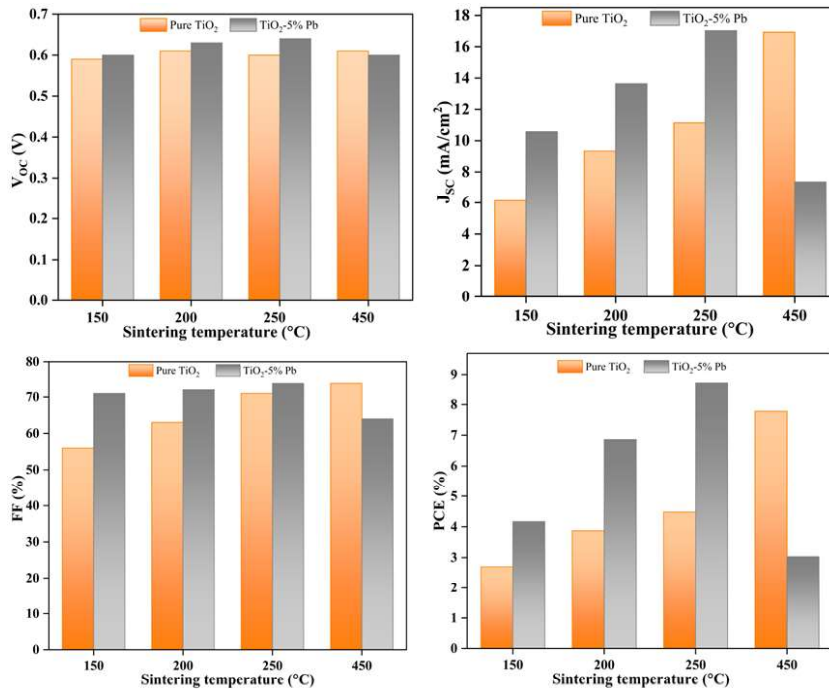


Figure 89: V_{OC} , J_{SC} , FF and $IPCEPCE$ at different sintering temperatures

Considering the aforementioned parameters' results, the ~~incident photo-power~~ conversion efficiency ($IPCEPCE$) of DSSCs have also been determined. As the V_{OC} , J_{SC} , and FF values increased, the $IPCEPCE$ value also been increased. The highest $IPCEPCE$ value obtained in the research was 8.73% for DSSC based on TiO₂-5% Pb photoanode sintered at 250°C. This value was even higher than control DSSC prepared with pure TiO₂ at ~~typically~~ high sintering temperature of 450°C with $IPCEPCE$ of 7.78%. Hence, highlighting the superiority in performance of the TiO₂-Pb photoanode despite the low sintering temperature. The improved interparticle connection due to the necking at the TiO₂-Pb interface during the liquid phase sintering process have been attributed as the main cause for such good performance. The yielded $IPCEPCE$ value have also been supported by the low R_{CT} value obtained in the EIS analysis. With lower R_{CT} , the electrons were easily transferred into the TiO₂ surface, enhancing the DSSC performance [33]. The nanocomposite photoanode have also shown the highest dye loading value of $1.17 \times 10^{-7}/\text{cm}^2$, indicating high light harvesting capability. Besides, DSSC sample based on TiO₂-5% Pb photoanode sintered at high temperature of 450°C has also been prepared for comparison purposes with the low temperature

Formatted: Font color: Accent 2

1
2
3
4
5
6
7 DSSC. The result showed that the PCE value for this sample to be lower at 3.03%. The decrease
8 in efficiency could be attributed to the oxidation of Pb in the TiO₂ matrix since the oxidation
9 temperature of Pb is around 450°C-640°C [38]. Apart from that, the high sintering temperature
10 has caused Pb to be completely melted and causing excessive liquid phase formation that
11 lowers the porosity of the photoanode [39]. Thus, lowering the dye absorption capability of the
12 photoanode and eventually lowers the performance of DSSC. Hence, the DSSC based on TiO₂-
13 5% Pb @ 250°C photoanode has the best performance that was even better than the
14 ~~typical control~~ DSSC device. These results in Figure 89 highlighted the advantage of liquid
15 phase sintering with Pb sintering aid addition method in yielding high performing DSSC even
16 at low sintering temperature.

21 4.0 Conclusions

22
23 The research aims to improve the efficiency of DSSC devices being prepared at
24 relatively lower sintering temperature. Metallic Pb particles as sintering aid has been employed
25 to reduce the sintering temperature of TiO₂ based photoanode. Various concentrations of Pb
26 from 0.5-10wt% has been tried at different sintering temperatures to optimise the electro-
27 optical properties. ~~FESEM, SEM-EDX, TEM and XRD have been employed to study the~~
28 ~~surface morphology, elemental composition and mapping, surface interaction and phase~~
29 ~~identification respectively. UV-vis has been used to examine the photo response of the as~~
30 ~~prepared specimens. Finally, EIS and solar simulator has been employed to study the charge~~
31 ~~transfer properties and conversion efficiency.~~ Increase in Pb concentration and temperature
32 leads to improved ~~IPCEPCE~~. This is due to improved ~~inter-partieleinterparticle~~ contact due to
33 surface fusion of Pb. DSSC prepared with TiO₂-5% Pb photoanode sintered at 250°C exhibited
34 highest ~~IPCEPCE~~ value of 8.73% surpassing even the high temperature DSSC control samples
35 by approximately 12.21% prepared with pure TiO₂ photoanode sintered at 450°C (~~IPCEPCE~~:
36 7.78%). The addition of Pb as sintering aid improved the ~~inter-partieleinterparticle~~ connection
37 leading to increased in current density and a reduction in recombination reactions. Further
38 increase in concentration of Pb did not improve the ~~IPCEPCE~~ which may be cor-related with
39 increased impurities in the TiO₂ matrix, which in turn leads to layer cracking and increased
40 charge trapping sites. Besides Pb, other metallic nanoparticles with low melting point should
41 also be researched in the future by using the liquid phase sintering applied in this research.
42 Metal nanoparticles with a lower melting point could produce highly efficient DSSC at lower
43 sintering temperatures that would be suitable for flexible DSSC substrate. The method has
44 shown to be effective for low sintering temperature operation, is a simple process and there is

Formatted: Font color: Accent 2

Formatted: Font color: Accent 2

Formatted: Font color: Accent 2

Formatted: Font color: Accent 2

1
2
3
4
5
6
7
8
9
10
11
12
13
14
15
16
17
18
19
20
21
22
23
24
25
26
27
28
29
30
31
32
33
34
35
36
37
38
39
40
41
42
43
44
45
46
47
48
49
50
51
52
53
54
55
56
57
58
59
60
61
62
63
64
65

1
2
3
4
5
6
7 wide availability of metal nanoparticles that are potentially suitable to be used for future
8 research.
9

10 11 **Acknowledgment**

12 The authors would like to acknowledge Ministry of Higher Education Malaysia for financial
13 assistance through Fundamental Research Grant Scheme (FRGS)
14 (FRGS/1/2020/STG05/SYUC/02/1)
15
16

17 18 **Declaration-of-interests**

19 The authors declare that they have no known competing financial interests or personal
20 relationships that could have influenced the work reported in this paper.
21
22

23 **References**

- 24
25 [1] K. Sharma, V. Sharma, S.S. Sharma, Dye-Sensitized Solar Cells: Fundamentals and
26 Current Status, Nanoscale Res Lett. 13 (2018) 381. [https://doi.org/10.1186/s11671-](https://doi.org/10.1186/s11671-018-2760-6)
27 018-2760-6.
- 28 [2] M.A. Saeed, K. Yoo, H.C. Kang, J.W. Shim, J.J. Lee, Recent developments in dye-
29 sensitized photovoltaic cells under ambient illumination, Dyes and Pigments. 194
30 (2021) 109626. <https://doi.org/10.1016/j.dyepig.2021.109626>.
- 31 [3] C. Wu, K. Wang, M. Batmunkh, A.S.R. Bati, D. Yang, Y. Jiang, Y. Hou, J.G. Shapter,
32 S. Priya, Multifunctional nanostructured materials for next generation photovoltaics,
33 Nano Energy. 70 (2020) 104480. <https://doi.org/10.1016/J.NANOEN.2020.104480>.
- 34 [4] M.S. Ahmad, A.K. Pandey, N. Abd Rahim, N. Aslfattahi, Y.K. Mishra, B. Rashid, R.
35 Saidur, 2-D Mxene flakes as potential replacement for both TCO and Pt layers for
36 Dye-Sensitized Solar cell, Ceram Int. 47 (2021) 27942–27947.
37 <https://doi.org/10.1016/j.ceramint.2021.06.225>.
- 38 [5] M.S. Ahmad, N.A. Rahim, Syed shahabuddin, S. Mehmood, A.D. Khan, Effect of
39 WS2 nano-sheets on the catalytic activity of polyaniline nano-rods based counter
40 electrode for dye sensitized solar cell, Physica E Low Dimens Syst Nanostruct. 126
41 (2021) 114466. <https://doi.org/10.1016/j.physe.2020.114466>.
- 42 [6] J.M. Ji, H. Zhou, Y.K. Eom, C.H. Kim, H.K. Kim, 14.2% Efficiency Dye-Sensitized
43 Solar Cells by Co-sensitizing Novel Thieno[3,2-b]indole-Based Organic Dyes with a
44 Promising Porphyrin Sensitizer, Adv Energy Mater. 10 (2020) 2000124.
45 <https://doi.org/10.1002/aenm.202000124>.
- 46 [7] A. Yella, H.W. Lee, H.N. Tsao, C. Yi, A.K. Chandiran, M.K. Nazeeruddin, E.W.G.
47 Diau, C.Y. Yeh, S.M. Zakeeruddin, M. Grätzel, Porphyrin-sensitized solar cells with
48 cobalt (II/III)-based redox electrolyte exceed 12 percent efficiency, Science (1979),
49 334 (2011) 629–634. <https://doi.org/10.1126/science.1209688>.
50
51
52
53
54
55
56
57
58
59
60
61
62
63
64
65

- 1
2
3
4
5
6
7
8
9
10
11
12
13
14
15
16
17
18
19
20
21
22
23
24
25
26
27
28
29
30
31
32
33
34
35
36
37
38
39
40
41
42
43
44
45
46
47
48
49
50
51
52
53
54
55
56
57
58
59
60
61
62
63
64
65
- [8] [H. Min, D.Y. Lee, J. Kim, G. Kim, K.S. Lee, J. Kim, M.J. Paik, Y.K. Kim, K.S. Kim, M.G. Kim, T.J. Shin, S. il Seok, Perovskite solar cells with atomically coherent interlayers on SnO₂ electrodes. *Nature* 2021 598:7881. 598 \(2021\) 444–450. <https://doi.org/10.1038/s41586-021-03964-8>.](#)
- [9] [Y. Cui, Y. Xu, H. Yao, P. Bi, L. Hong, J. Zhang, Y. Zu, T. Zhang, J. Qin, J. Ren, Z. Chen, C. He, X. Hao, Z. Wei, J. Hou, Single-Junction Organic Photovoltaic Cell with 19% Efficiency. *Advanced Materials*. 33 \(2021\) 2102420. <https://doi.org/10.1002/ADMA.202102420>.](#)
- [10] [R. Zhu, Z. Zhang, Y. Li, Advanced materials for flexible solar cell applications. *Nanotechnol Rev.* 8 \(2019\) 452–458. <https://doi.org/10.1515/ntrev-2019-0040>.](#)
- [11] [G. Li, L. Sheng, T. Li, J. Hu, P. Li, K. Wang, Engineering flexible dye-sensitized solar cells for portable electronics. *Solar Energy*. 177 \(2019\) 80–98. <https://doi.org/10.1016/J.SOLENER.2018.11.017>.](#)
- [12] [N.S. Noorasid, F. Arith, A.N. Mustafa, M.A. Azam, S. Mahalingam, P. Chelvanathan, N. Amin, Current advancement of flexible dye sensitized solar cell: A review. *Optik \(Stuttg\)*. 254 \(2022\) 168089. <https://doi.org/10.1016/j.ijleo.2021.168089>.](#)
- [13] [J. Zhang, Z. Wang, X. Li, J. Yang, C. Song, Y. Li, J. Cheng, Q. Guan, B. Wang, Flexible Platinum-Free Fiber-Shaped Dye Sensitized Solar Cell with 10.28% Efficiency. *ACS Appl Energy Mater.* 2 \(2019\) 2870–2877. <https://doi.org/10.1021/acsaem.9b00207>.](#)
- [14] [H. Khir, A.K. Pandey, R. Saidur, M. Shakeel Ahmad, N. Abd Rahim, M. Dewika, M. Samykano, Recent advancements and challenges in flexible low temperature dye sensitised solar cells. *Sustainable Energy Technologies and Assessments*. 53 \(2022\) 102745. <https://doi.org/10.1016/J.SETA.2022.102745>.](#)
- [15] [M.E. Yeoh, K.Y. Chan, Recent advances in photo-anode for dye-sensitized solar cells: a review. *Int J Energy Res.* 41 \(2017\) 2446–2467. <https://doi.org/10.1002/er.3764>.](#)
- [16] [S. Ni, F. Guo, D. Wang, S. Jiao, J. Wang, Y. Zhang, B. Wang, P. Feng, L. Zhao, Modification of TiO₂ nanowire arrays with Sn doping as photoanode for highly efficient dye-sensitized solar cells. *Crystals \(Basel\)*. 9 \(2019\) 113. <https://doi.org/10.3390/cryst9020113>.](#)
- [17] [R.S. Dubey, S.R. Jadkar, A.B. Bhorde, Synthesis and Characterization of Various Doped TiO₂ Nanocrystals for Dye-Sensitized Solar Cells. *ACS Omega*. 6 \(2021\) 3470–3482. <https://doi.org/10.1021/acsomega.0c01614>.](#)
- [18] [L. Song, J. Zhai, P. Du, J. Xiong, F. Ko, A novel bilayer photoanode made of carbon nanotubes incorporated TiO₂ nanorods and Mg²⁺ doped TiO₂ nanorods for flexible dye-sensitized solar cells. *Thin Solid Films*. 646 \(2018\) 44–52. <https://doi.org/10.1016/j.tsf.2017.11.030>.](#)
- [19] [R. de Oro Calderon, C. Gierl-Mayer, H. Danninger, Fundamentals of Sintering: Liquid Phase Sintering. *Encyclopedia of Materials: Metals and Alloys*. 3 \(2022\) 481–492. <https://doi.org/10.1016/B978-0-12-819726-4.00127-7>.](#)

- 1
2
3
4
5
6
7
8
9
10
11
12
13
14
15
16
17
18
19
20
21
22
23
24
25
26
27
28
29
30
31
32
33
34
35
36
37
38
39
40
41
42
43
44
45
46
47
48
49
50
51
52
53
54
55
56
57
58
59
60
61
62
63
64
65
- [20] M.S. Ahmad, N.A. Rahim, A.K. Pandey, Improved electron transfer of TiO₂ based dye sensitized solar cells using Ge as sintering aid, *Optik (Stuttg)*. 157 (2018) 134–140. <https://doi.org/10.1016/j.ijleo.2017.11.073>.
- [21] M.S. Ahmad, A.K. Pandey, N.A. Rahim, S. Shahabuddin, S.K. Tyagi, Chemical sintering of TiO₂ based photoanode for efficient dye sensitized solar cells using Zn nanoparticles, *Ceram Int*. 44 (2018) 18444–18449. <https://doi.org/10.1016/j.ceramint.2018.07.062>.
- [22] P.S. Liu, G.F. Chen, Making Porous Metals, in: *Porous Materials - Processing and Applications*, Elsevier, 2014: pp. 21–112. <https://doi.org/10.1016/b978-0-12-407788-1.00002-2>.
- [23] A. Mallick, I. Visoly-Fisher, Pb in halide perovskites for photovoltaics: Reasons for optimism, *Mater Adv*. 2 (2021) 6125–6135. <https://doi.org/10.1039/d1ma00355k>.
- [24] R. Long, Y. Dai, G. Meng, B. Huang, Energetic and electronic properties of X- (Si, Ge, Sn, Pb) doped TiO₂ from first-principles, *Physical Chemistry Chemical Physics*. 11 (2009) 8165–8172. <https://doi.org/10.1039/b903298c>.
- [25] H. Khan, Y. Iqbal, M. Khan, S.N. Ahmad, Y. Zeng, Variations in the optical properties of TiO₂ with Pb doping using ab initio calculations, *Int J Mod Phys B*. 35 (2021) 29. <https://doi.org/10.1142/S0217979221502969>.
- [26] A.K. Mishra, S. Saha, FABRICATION AND CHARACTERIZATION OF NATURAL DYE SENSITIZED SOLAR CELLS BASED ON PbS NANOSTRUCTURES, *Chalcogenide Letters*. 17 (2020) 605–614. https://chalcogen.ro/605_MishraAK.pdf (accessed September 7, 2022).
- [27] R. Singh, S.P. Pandey, P.K. Shukla, S.K. Tomar, B. Bhattacharya, P.K. Singh, Synthesis of lead sulphide nanoparticles for electrode application of dye sensitized solar cells, *Nanoscience and Nanotechnology Letters*. 6 (2014) 31–36. <https://doi.org/10.1166/nnl.2014.1722>.
- [28] J. Jia, H. Yamamoto, T. Okajima, Y. Shigesato, On the Crystal Structural Control of Sputtered TiO₂ Thin Films, *Nanoscale Res Lett*. 11 (2016) 324. <https://doi.org/10.1186/s11671-016-1531-5>.
- [29] J. He, Y. en Du, Y. Bai, J. An, X. Cai, Y. Chen, P. Wang, X. Yang, Q. Feng, Facile formation of anatase/rutile TiO₂ nanocomposites with enhanced photocatalytic activity, *Molecules*. 24 (2019) 2996. <https://doi.org/10.3390/molecules24162996>.
- [30] F. Scarpelli, T.F. Mastropietro, T. Poerio, N. Godbert, Mesoporous TiO₂ Thin Films: State of the Art, in: *Titanium Dioxide - Material for a Sustainable Environment*, InTech, 2018: pp. 57–80. <https://doi.org/10.5772/intechopen.74244>.
- [31] Q. Zhang, C. Li, High temperature stable anatase phase titanium dioxide films synthesized by mist chemical vapor deposition, *Nanomaterials*. 10 (2020) 911. <https://doi.org/10.3390/nano10050911>.
- [32] F. Gontad, A. Lorusso, A. Klini, A. Loufardaki, M. Panareo, C. Fotakis, A. Perrone, Picosecond and subpicosecond pulsed laser deposition of Pb thin films, *Physical*

1
2
3
4
5
6
7 [Review Special Topics - Accelerators and Beams. 16 \(2013\).
https://doi.org/10.1103/PhysRevSTAB.16.093401.](https://doi.org/10.1103/PhysRevSTAB.16.093401)

- 8
9
10 [33] [G.A. Alamu, O. Adedokun, I.T. Bello, Y.K. Sanusi, Plasmonic enhancement of visible
light absorption in Ag-TiO₂ based dye-sensitized solar cells, Chemical Physics Impact.
3 \(2021\) 100037. https://doi.org/10.1016/J.CHPHI.2021.100037.](https://doi.org/10.1016/J.CHPHI.2021.100037)
- 11
12
13 [34] [P. Pandey, M.R. Parra, F.Z. Haque, R. Kurchania, Effects of annealing temperature
optimization on the efficiency of ZnO nanoparticles photoanode based dye sensitized
solar cells, Journal of Materials Science: Materials in Electronics. 28 \(2017\) 1537–
1545. https://doi.org/10.1007/s10854-016-5693-9.](https://doi.org/10.1007/s10854-016-5693-9)
- 14
15
16 [35] [B. O'Regan, M. Gratzel, A low-cost, high-efficiency solar cell based on dye-sensitized
colloidal TiO₂ films, Nature. 353 \(1991\) 737–740.
https://doi.org/https://doi.org/10.1038/353737a0.](https://doi.org/10.1038/353737a0)
- 17
18
19 [36] [K.G. Baiju, B. Murali, R. Subba Rao, K. Jayanarayanan, D. Kumaresan, Heat sink
assisted elevated temperature sintering process of TiO₂ on polymer substrates for
producing high performance flexible dye-sensitized solar cells, Chemical Engineering
and Processing - Process Intensification. 149 \(2020\) 107817.
https://doi.org/10.1016/j.cep.2020.107817.](https://doi.org/10.1016/j.cep.2020.107817)
- 20
21
22 [37] [S.N.F. Zainudin, H. Abdullah, M. Markom, Electrochemical studies of tin oxide
based-dye-sensitized solar cells \(DSSC\): a review, Journal of Materials Science:
Materials in Electronics. 30 \(2019\) 5342–5356. https://doi.org/10.1007/s10854-019-
00929-6.](https://doi.org/10.1007/s10854-019-00929-6)
- 23
24
25 [38] [T.E. Weyand, The oxidation kinetics of liquid lead and lead alloys, DOCTORAL
DISSERTATIONS, University of Missouri, 1970.
https://scholarsmine.mst.edu/doctoral_dissertations/2042.](https://scholarsmine.mst.edu/doctoral_dissertations/2042)
- 26
27
28 [39] [A. Sabahi Namini, M. Azadbeh, A. Mohammadzadeh, Microstructure and
densification behavior of liquid phase sintered Cu-28Zn prealloyed powder, Science of
Sintering. 45 \(2013\) 351–362. https://doi.org/10.2298/SOS1303351S.](https://doi.org/10.2298/SOS1303351S)
- 29
30
31 [1] [K. Sharma, V. Sharma, S.S. Sharma, Dye-Sensitized Solar Cells: Fundamentals and
Current Status, Nanoscale Res Lett. 13 \(2018\) 381. https://doi.org/10.1186/s11671-
018-2760-6.](https://doi.org/10.1186/s11671-018-2760-6)
- 32
33
34 [2] [M.A. Saeed, K. Yoo, H.C. Kang, J.W. Shim, J.J. Lee, Recent developments in dye-
sensitized photovoltaic cells under ambient illumination, Dyes and Pigments. 194
\(2021\) 109626. https://doi.org/10.1016/j.dyepig.2021.109626.](https://doi.org/10.1016/j.dyepig.2021.109626)
- 35
36
37 [3] [C. Wu, K. Wang, M. Batmunkh, A.S.R. Bati, D. Yang, Y. Jiang, Y. Hou, J.G. Shapter,
S. Priya, Multifunctional nanostructured materials for next generation photovoltaics,
Nano Energy. 70 \(2020\) 104480. https://doi.org/10.1016/J.NANOEN.2020.104480.](https://doi.org/10.1016/J.NANOEN.2020.104480)
- 38
39
40 [4] [M.S. Ahmad, A.K. Pandey, N. Abd Rahim, N. Aslfattahi, Y.K. Mishra, B. Rashid, R.
Saidur, 2-D Mxene flakes as potential replacement for both TCO and Pt layers for
Dye Sensitized Solar cell, Ceram Int. 47 \(2021\) 27942–27947.
https://doi.org/10.1016/j.ceramint.2021.06.225.](https://doi.org/10.1016/j.ceramint.2021.06.225)
- 41
42
43
44
45
46
47
48
49
50
51
52
53
54
55
56
57
58
59
60
61
62
63
64
65

- 1
2
3
4
5
6
7
8
9
10
11
12
13
14
15
16
17
18
19
20
21
22
23
24
25
26
27
28
29
30
31
32
33
34
35
36
37
38
39
40
41
42
43
44
45
46
47
48
49
50
51
52
53
54
55
56
57
58
59
60
61
62
63
64
65
- [5] M.S. Ahmad, N.A. Rahim, Syed shahabuddin, S. Mehmood, A.D. Khan, Effect of WS₂ nano sheets on the catalytic activity of polyaniline nano rods based counter electrode for dye sensitized solar cell, *Physica E Low Dimens Syst Nanostruct.* 126 (2021) 114466. <https://doi.org/10.1016/j.physe.2020.114466>.
- [6] J.M. Ji, H. Zhou, Y.K. Eom, C.H. Kim, H.K. Kim, 14.2% Efficiency Dye Sensitized Solar Cells by Co-sensitizing Novel Thieno[3,2-b]indole Based Organic Dyes with a Promising Porphyrin Sensitizer, *Adv Energy Mater.* 10 (2020) 2000124. <https://doi.org/10.1002/aenm.202000124>.
- [7] A. Yella, H.W. Lee, H.N. Tsao, C. Yi, A.K. Chandiran, M.K. Nazeeruddin, E.W.G. Diau, C.Y. Yeh, S.M. Zakeeruddin, M. Grätzel, Porphyrin sensitized solar cells with cobalt (II/III) based redox electrolyte exceed 12 percent efficiency, *Science* (1979). 334 (2011) 629–634. <https://doi.org/10.1126/science.1209688>.
- [8] H. Min, D.Y. Lee, J. Kim, G. Kim, K.S. Lee, J. Kim, M.J. Paik, Y.K. Kim, K.S. Kim, M.G. Kim, T.J. Shin, S. il Seok, Perovskite solar cells with atomically coherent interlayers on SnO₂ electrodes, *Nature* 2021 598:7881. 598 (2021) 444–450. <https://doi.org/10.1038/s41586-021-03964-8>.
- [9] Y. Cui, Y. Xu, H. Yao, P. Bi, L. Hong, J. Zhang, Y. Zu, T. Zhang, J. Qin, J. Ren, Z. Chen, C. He, X. Hao, Z. Wei, J. Hou, Single Junction Organic Photovoltaic Cell with 19% Efficiency, *Advanced Materials.* 33 (2021) 2102420. <https://doi.org/10.1002/ADMA.202102420>.
- [10] R. Zhu, Z. Zhang, Y. Li, *Advanced materials for flexible solar cell applications, Nanotechnol Rev.* 8 (2019) 452–458. <https://doi.org/10.1515/ntrev-2019-0040>.
- [11] G. Li, L. Sheng, T. Li, J. Hu, P. Li, K. Wang, Engineering flexible dye sensitized solar cells for portable electronics, *Solar Energy.* 177 (2019) 80–98. <https://doi.org/10.1016/j.solener.2018.11.017>.
- [12] N.S. Nooraid, F. Arith, A.N. Mustafa, M.A. Azam, S. Mahalingam, P. Chelvanathan, N. Amin, Current advancement of flexible dye sensitized solar cell: A review, *Optik (Stuttg).* 254 (2022) 168089. <https://doi.org/10.1016/j.ijleo.2021.168089>.
- [13] J. Zhang, Z. Wang, X. Li, J. Yang, C. Song, Y. Li, J. Cheng, Q. Guan, B. Wang, Flexible Platinum-Free Fiber Shaped Dye Sensitized Solar Cell with 10.28% Efficiency, *ACS Appl Energy Mater.* 2 (2019) 2870–2877. <https://doi.org/10.1021/acsaem.9b00207>.
- [14] H. Khir, A.K. Pandey, R. Saidur, M. Shakeel Ahmad, N. Abd Rahim, M. Dewika, M. Samykano, Recent advancements and challenges in flexible low temperature dye sensitised solar cells, *Sustainable Energy Technologies and Assessments.* 53 (2022) 102745. <https://doi.org/10.1016/j.seta.2022.102745>.
- [15] M.E. Yeoh, K.Y. Chan, Recent advances in photo-anode for dye sensitized solar cells: a review, *Int J Energy Res.* 41 (2017) 2446–2467. <https://doi.org/10.1002/er.3764>.
- [16] S. Ni, F. Guo, D. Wang, S. Jiao, J. Wang, Y. Zhang, B. Wang, P. Feng, L. Zhao, Modification of TiO₂ nanowire arrays with Sn doping as photoanode for highly

efficient dye sensitized solar cells, *Crystals (Basel)*. 9 (2019) 113.
<https://doi.org/10.3390/cryst9020113>.


- [17] R.S. Dubey, S.R. Jadhkar, A.B. Bhorde, Synthesis and Characterization of Various Doped TiO₂ Nanocrystals for Dye Sensitized Solar Cells, *ACS Omega*. 6 (2021) 3470–3482. <https://doi.org/10.1021/acsomega.0c01614>.
- [18] L. Song, J. Zhai, P. Du, J. Xiong, F. Ke, A novel bilayer photoanode made of carbon nanotubes incorporated TiO₂ nanorods and Mg²⁺ doped TiO₂ nanorods for flexible dye sensitized solar cells, *Thin Solid Films*. 646 (2018) 44–52.
<https://doi.org/10.1016/j.tsf.2017.11.030>.
- [19] R. de Oro Calderon, C. Gierl Mayer, H. Danninger, Fundamentals of Sintering: Liquid Phase Sintering, in: *Encyclopedia of Materials: Metals and Alloys*, Elsevier, 2021: pp. 481–492. <https://doi.org/10.1016/B978-0-12-819726-4.00127-7>.
- [20] M.S. Ahmad, N.A. Rahim, A.K. Pandey, Improved electron transfer of TiO₂ based dye sensitized solar cells using Ge as sintering aid, *Optik (Stuttg)*. 157 (2018) 134–140. <https://doi.org/10.1016/j.ijleo.2017.11.073>.
- [21] M.S. Ahmad, A.K. Pandey, N.A. Rahim, S. Shahabuddin, S.K. Tyagi, Chemical sintering of TiO₂ based photoanode for efficient dye sensitized solar cells using Zn nanoparticles, *Ceram Int*. 44 (2018) 18444–18449.
<https://doi.org/10.1016/j.ceramint.2018.07.062>.
- [22] P.S. Liu, G.F. Chen, Making Porous Metals, in: *Porous Materials—Processing and Applications*, Elsevier, 2014: pp. 21–112. <https://doi.org/10.1016/b978-0-12-407788-1.00002-2>.
- [23] H. Abadin, A. Ashizawa, Y. W. Stevens, F. Llados, G. Diamond, G. Sage, M. Citra, A. Quinones, S.J. Bosch, S.G. Swarts, Chemical and Physical Information, in: *Toxicological Profile for Lead*, Agency for Toxic Substances and Disease Registry (US), Atlanta, GA, 2007: pp. 277–288.
<https://www.ncbi.nlm.nih.gov/books/NBK158769/> (accessed September 7, 2022).
- [24] R. Long, Y. Dai, G. Meng, B. Huang, Energetic and electronic properties of X (Si, Ge, Sn, Pb) doped TiO₂ from first principles, *Physical Chemistry Chemical Physics*. 11 (2009) 8165–8172. <https://doi.org/10.1039/b903298e>.
- [25] J. Yu, J.C. Yu, B. Cheng, X. Zhao, Photocatalytic activity and characterization of the sol-gel derived Pb doped TiO₂ thin films, *J Solgel Sci Technol*. 24 (2002) 39–48.
<https://doi.org/10.1023/A:1015109515825>.
- [26] A.K. Mishra, S. Saha, FABRICATION AND CHARACTERIZATION OF NATURAL DYE SENSITIZED SOLAR CELLS BASED ON PbS NANOSTRUCTURES, *Chalcogenide Letters*. 17 (2020) 605–614.
https://chalcogen.ro/605_MishraAK.pdf (accessed September 7, 2022).
- [27] R. Singh, S.P. Pandey, P.K. Shukla, S.K. Tomar, B. Bhattacharya, P.K. Singh, Synthesis of lead sulphide nanoparticles for electrode application of dye sensitized solar cells, *Nanoscience and Nanotechnology Letters*. 6 (2014) 31–36.
<https://doi.org/10.1166/nnl.2014.1722>.

- 1
2
3
4
5
6
7
8 [28] J. Jia, H. Yamamoto, T. Okajima, Y. Shigesato, On the Crystal Structural Control of
9 Sputtered TiO₂ Thin Films, *Nanoscale Res Lett.* 11 (2016) 324.
10 <https://doi.org/10.1186/s11671-016-1531-5>.
- 11 [29] J. He, Y. en Du, Y. Bai, J. An, X. Cai, Y. Chen, P. Wang, X. Yang, Q. Feng, Facile
12 formation of anatase/rutile TiO₂ nanocomposites with enhanced photocatalytic
13 activity, *Molecules.* 24 (2019) 2996. <https://doi.org/10.3390/molecules24162996>.
- 14 [30] F. Scarpelli, T.F. Mastropietro, T. Poerio, N. Godbert, Mesoporous TiO₂ Thin Films:
15 State of the Art, in: *Titanium Dioxide—Material for a Sustainable Environment*,
16 InTech, 2018: pp. 57–80. <https://doi.org/10.5772/intechopen.74244>.
- 17 [31] Q. Zhang, C. Li, High temperature stable anatase phase titanium dioxide films
18 synthesized by mist chemical vapor deposition, *Nanomaterials.* 10 (2020) 911.
19 <https://doi.org/10.3390/nano10050911>.
- 20 [32] F. Gontad, A. Lorusso, A. Klini, A. Loufardaki, M. Panareo, C. Fotakis, A. Perrone,
21 Picosecond and subpicosecond pulsed laser deposition of Pb thin films, *Physical*
22 *Review Special Topics—Accelerators and Beams.* 16 (2013).
23 <https://doi.org/10.1103/PhysRevSTAB.16.093401>.
- 24 [33] M. Balakrishnan, R. John, Impact of Ni metal ion concentration in TiO₂ nanoparticles
25 for enhanced photovoltaic performance of dye sensitized solar Cell, *Journal of*
26 *Materials Science: Materials in Electronics.* 32 (2021) 5295–5308.
27 <https://doi.org/10.1007/s10854-020-05100-0>.
- 28 [34] P. Pandey, M.R. Parra, F.Z. Haque, R. Kurchania, Effects of annealing temperature
29 optimization on the efficiency of ZnO nanoparticles photoanode based dye sensitized
30 solar cells, *Journal of Materials Science: Materials in Electronics.* 28 (2017) 1537–
31 1545. <https://doi.org/10.1007/s10854-016-5693-9>.
- 32 [35] B. O'Regan, M. Gratzel, A low-cost, high-efficiency solar cell based on dye sensitized
33 colloidal TiO₂ films, *Nature.* 353 (1991) 737–740.
34 <https://doi.org/https://doi.org/10.1038/353737a0>.
- 35 [36] S.N.F. Zainudin, H. Abdullah, M. Markom, Electrochemical studies of tin oxide
36 based dye sensitized solar cells (DSSC): a review, *Journal of Materials Science:*
37 *Materials in Electronics.* 30 (2019) 5342–5356. <https://doi.org/10.1007/s10854-019-00929-6>.
- 38
39
40
41
42
43
44
45
46
47
48
49
50
51
52
53
54
55
56
57
58
59
60
61
62
63
64
65

Declaration of interests

The authors declare that they have no known competing financial interests or personal relationships that could have appeared to influence the work reported in this paper.

The authors declare the following financial interests/personal relationships which may be considered as potential competing interests:



Dr. Adarsh Kumar Pandey
Professor and Program Leader
Research Centre for Nano-Materials & Energy Technology
School of Engineering and Technology, Sunway University, Malaysia
Corresponding Author
Email: adarsh.889@gmail.com; adarshp@sunway.edu.my